

Efficient Continual Learning Ensembles in Neural Network Subspaces

Thang Doan^{*1}, Seyed Iman Mirzadeh², Joelle Pineau¹, and Mehrdad Farajtabar³

¹McGill / Mila, ²Washington State University, ³DeepMind

Abstract

A growing body of research in continual learning focuses on the catastrophic forgetting problem. While many attempts have been made to alleviate this problem, the majority of the methods assume a *single model* in the continual learning setup. In this work, we question this assumption and show that employing *ensemble models* can be a simple yet effective method to improve continual performance. However, the training and inference cost of ensembles can increase linearly with the number of models. Motivated by this limitation, we leverage the recent advances in the deep learning optimization literature, such as mode connectivity and neural network subspaces, to derive a new method that is both computationally advantageous and can outperform the state-of-the-art continual learning algorithms.

1 Introduction

Continual learning (CL) and Lifelong learning (Thrun, 1994) have recently gained popularity since many real-world applications fall into that setting. It describes the scenario where not only a stream of data arrives sequentially, but their distribution also shifts over time. This setup induces Catastrophic Forgetting (CF) (McCloskey and Cohen, 1989) which is a degradation of performances on previous data due to distribution change between tasks (Doan et al., 2021).

One fundamental goal in continual learning is to learn from the new incoming tasks while retaining knowledge from the past and avoiding interference that can lead to poor performance (Lesort et al., 2021). This becomes particularly challenging when facing a long heterogeneous stream of data because all the burden is left to a single model, as shown in Fig. 1 (left). A simple yet effective solution is to rely on an ensemble method, as shown in Fig. 1 (middle), that improves performance over a single model. It's well known that ensemble methods perform well in supervised learning (Dietterich, 2000), however, their functionality is barely studied in the continual learning setting.

Inspired by bootstrapping (Breiman, 1996), deep ensembles initialize and train multiple neural networks independently (Lakshminarayanan et al., 2017; Fort et al., 2019). Not only does this improve their robustness, but it also boosts the overall performance thanks to a higher diversity in the solutions and their de-correlated predictions (Goodfellow et al., 2014b; Havasi et al., 2020). This simple mechanism allows ensemble methods to improve performance over single models (Huang et al., 2017).

In the context of continual learning, using an ensemble method and having diversity in the solutions allows each model to specialize in different tasks (see Fig. 2). Given that only some of the individual

^{*}Correspondence to thang.doan@mail.mcgill.ca

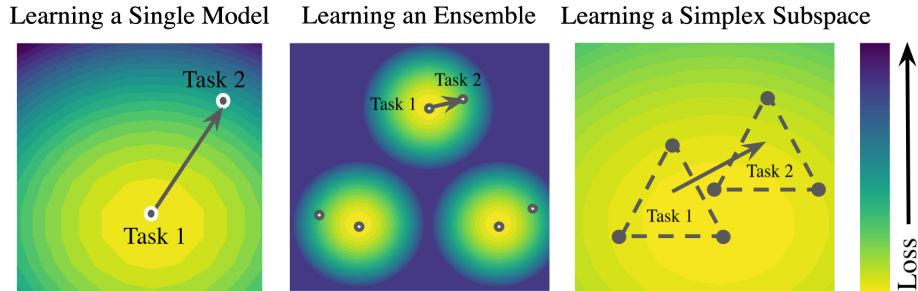


Figure 1: **(left)** In standard training, we learn a single model as a solution and there is no restriction on parameter movement. **(middle)** An ensemble uses multiple independently trained models. While this can improve performance it will be computationally expensive. **(right)** By learning a low-loss subspace, which is as cheap as learning a single model, we can learn robust solutions.

models may need a drastic or a slight change to learn the incoming tasks, it leads to an attenuation of forgetting and a boost in the overall performance (Fig. 3a). A similar observation has been made recently by Caccia et al. (2021) in their “anytime learning” framework where data arrive by batches instead of a whole dataset.

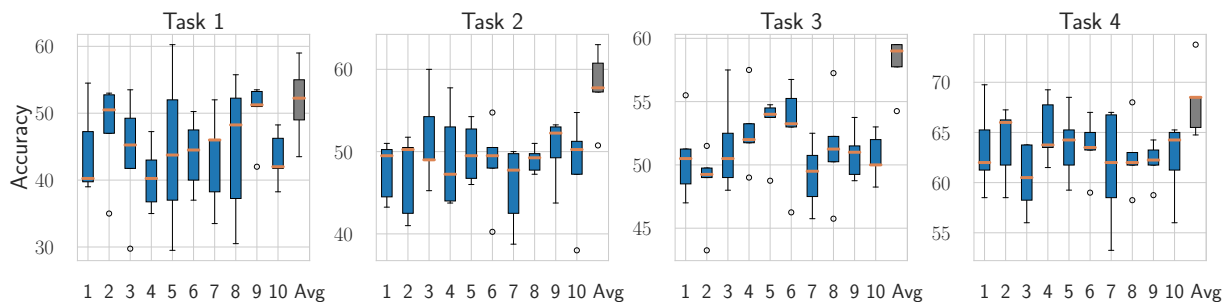


Figure 2: Final accuracy for each of the 10 members of the ensemble (blue) and the final ensemble model (gray) for Split CIFAR-100. The final ensemble prediction accuracy is almost always higher than the accuracy of the best model. Moreover, each model specializes in different tasks throughout the training contributing to the performance of the ensemble method.

However, the computational cost of ensembles grows linearly with the number of models (see Fig. 3b). This limits their usage for real-world applications due to computational or environmental concerns. Consider edge or mobile devices or wearable embodied AI as examples, where not only must the inference be carried on-device, but there is also a need to train an always-on AI model that continually learns while interacting with the user or perceiving the world (Manolis Savva* et al., 2019; Szot et al., 2021).

While it is possible to focus solely on the computational cost problem to find an efficient parameter sharing algorithm Wen et al. (2020), in this work, we focus on both the computational efficiency and accuracy performance. Our work is motivated by the recent advances in the deep learning optimization literature such as Neural Network Subspace (Wortsman et al., 2021) and Mode Connectivity (Garipov et al., 2018; Draxler et al., 2018; Mirzadeh et al., 2021b). Instead of working with an ensemble of independent networks (ensemble method), we consider the subspace of their convex combination as a viable set of solutions and show that their center is more robust to forgetting. To further overcome CF over the continual learning experience, we connect the subspaces learned via regions of low loss. These subspaces tie the weights of all the individual models together allowing mitigation of the CF while being able to learn new tasks. As illustrated in Fig. 1 (right), learning a subspace can lead to wider minima with the interpolation subspace between all models having a low loss. We also show that with a roughly similar computational cost as

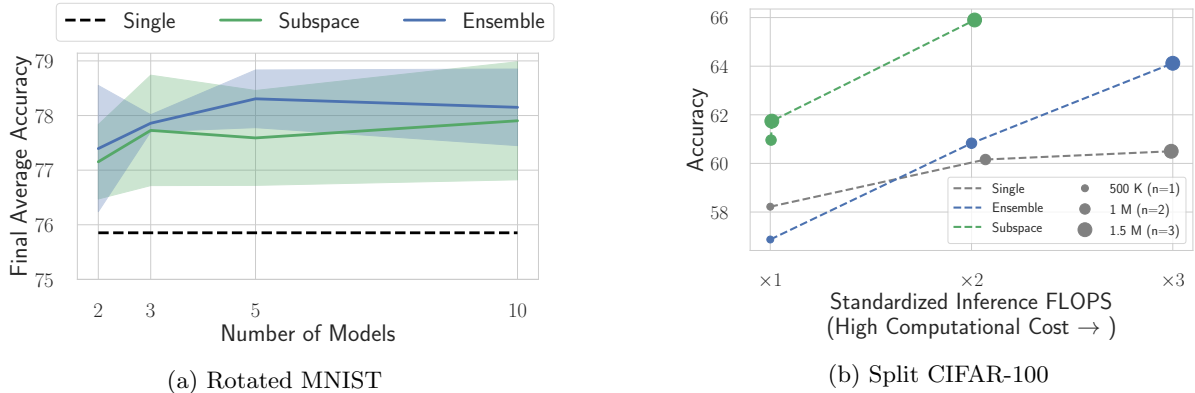


Figure 3: Having more than one model improves accuracy performance over single model (black dashed line) (**left**). The trade-off between computational cost and performance for Single model, Ensemble, and Subspace methods with an increasing number of parameters and number of models n . The x-axis represents how many times more compute (w.r.t to the single model) is needed to train the given model. While ensemble methods incur linear computational cost growth, subspace methods enjoy the same computational cost as a single model. Note that increasing the parameters of a single model does not necessarily improve its performance compared to ensemble methods (**right**).

training a single model, we can continually learn subspaces of low-loss solutions with multiple models.

Contributions. (a) We study continual learning with multiple models (ensemble and subspace methods) and showcase their benefits over single models for learning with varying data distribution. We show that ensemble methods rely on the diversity of its members to mitigate CF and boost performance (Sec. 3). (b) The latter implying high compute cost, we instead learn a low-loss subspaces of neural networks as a computationally efficient alternative for improving performance and robustness (Sec. 3). (c) Finally, we study the implications of using neural subspaces in continual learning and propose an efficient algorithm (Sec. 4) that outperforms state-of-the-art CL baselines (Sec. 5).

2 Preliminaries

2.1 Continual Learning (CL)

Let \mathcal{X} be some features and \mathcal{Y} the labels space ($\mathcal{Y} = \mathbb{R}$ for a regression problem and $\mathcal{Y} \in \Delta^K$ for classification problem¹). In CL, a stream of supervised learning tasks indexed by $\tau \in [T]$, \mathcal{T}_τ , (where $T \in \mathbb{N}^*$ is the total number of tasks) arrives sequentially. The goal is to learn a predictor $f_\omega : \mathcal{X} \times \mathcal{T} \rightarrow \mathcal{Y}$ (where $\omega \in \mathbb{R}^p$ are the learnable parameters of size p) that performs a prediction as accurate as possible with respect to a loss function \mathcal{L}_τ . We denote the weight learned after task τ as ω_τ^* . In the framework of CL, one cannot recover samples from previous tasks unless storing them in a replay buffer (Chaudhry et al., 2019b). A pseudo-code of the Vanilla Continual Learning Algorithm (single model) is provided in Appendix (Alg. 2).

¹ Δ^K denotes the vertices of the K -dim probability simplex

2.2 Training Ensemble Models for Continual Learning

In this work, we adapt the learning of ensemble methods to continual learning scenarios. Unless mentioned, we use the standard training procedure, which consists of training independently each of the n models on the same dataset². Given a set of weights $\{\omega_i\}_{i=1}^n$, a task τ , when a data batch (x, y) arrives, we optimize $\frac{1}{n} \sum_{i=1}^n \mathcal{L}_\tau(f_{\omega_i}(x), y)$. Therefore, the models' training differs only in the weights initialization of each model. The average prediction of each model is used as the output of the ensemble for evaluation $(\frac{1}{n} \sum_{i=1}^n f_{\omega_i}(\cdot))$ ³. That being said, the training cost simply grows linearly with the number of models n . A pseudo-code of the Ensemble CL Algorithm is provided in Alg. 3 in the Appendix.

2.3 Learning a Subspace Solution for CL

For the subspace method training, we proceed similarly as in Wortsman et al. (2021). Given a predictor f , a set of n learnable parameters $\{\omega_i\}_{i=1}^n$, learning a subspace of dimension n consists in training the predictor $f_{\bar{\omega}}$ as accurate as possible (with $\bar{\omega} = \sum_{i=1}^n \alpha_i \omega_i$, $\alpha \in \Delta^n$). Simply put, given a task τ , when a data batch (x, y) arrives, we optimize $\mathcal{L}_\tau(f_{\bar{\omega}}(x), y)$ where $\bar{\omega} = \sum_{i=1}^n \alpha_i \omega_i$, with $\alpha \sim \mathcal{U}(\Delta^n)$. Although, one can learn a distribution over the α 's, we consider the standard case like in Wortsman et al. (2020) where we sample it uniformly in the simplex Δ^n . The prediction steps differs only in the choice of α and will be discussed in the following sections. A pseudo-code of the Subspace Continual Learning Algorithm is provided in Alg. 4 in the Appendix.

When it comes to backpropagation, subspace methods enjoy slightly similar computation cost as the single model. Given a loss \mathcal{L} , the update w.r.t. each ω_i , is (assuming standard SGD optimizer): $\frac{\partial \mathcal{L}}{\partial \omega_i} = \frac{\partial \mathcal{L}}{\partial \bar{\omega}} \frac{\partial \bar{\omega}}{\partial \omega_i} = \alpha_i \frac{\partial \mathcal{L}}{\partial \bar{\omega}}$, $\forall i = 1 \dots n$. Then, only a *unique* backpropagation through the model f (w.r.t. to $\bar{\omega}$) is needed. A detailed discussion about the computational cost implication between ensemble and subspace methods is provided in Appendix B.

3 Continual Learning Beyond a Single Model

This section aims to provide the benefits of having more than one model for continual learning (whether it is an ensemble or a subspace method). To this end, we compare the merits and flaws of both methods. We first provide the experimental setting of our ablation analysis.

3.1 Experimental Setup

For the next section's ablation analysis, we will be using the following setup:

Benchmarks. For this ablation, we use two standard benchmarks following Goodfellow et al. (2014a), and Chaudhry et al. (2019b). Rotated MNIST (Farahtabar et al., 2020) consists of a series of MNIST classification tasks, where the images are rotated with respect to a fixed angle, monotonically. We increment the rotation angle by 22 degrees at each new task like in Mirzadeh et al. (2021b) to worsen the catastrophic forgetting phenomenon. Split CIFAR-100 (Chaudhry et al., 2019b) is constructed by splitting the original CIFAR-100 dataset (Krizhevsky et al., 2009) into 20 disjoint subsets, where each subset is formed by sampling without replacement of 5 classes out of 100. For the sake of our experiment, we fine-tune on a sequence of 5 tasks for each benchmark, seeing the tasks only once without relying on a replay buffer. While for brevity, we include the main results in this section, more detailed plots can be found in Appendix D.

²We also compare against bagging strategy in Appendix F.2.

³Classical majority voting strategies has been tried without significant difference in performance

Architectures. The neural networks architectures used are respectively fully connected layers with two hidden layers of 100 hidden units (Rotated MNIST) and a reduced Resnet-18 with three times fewer filters map across all layers as in (Mirzadeh et al., 2020b).

Metrics. To assess the performance of each baseline, we report the Final Accuracy and Forgetting Measure defined as follows. The Final Accuracy after T tasks is the average validation accuracy over all the tasks $\tau = 1 \dots T$ defined as: $A_T = \frac{1}{T} \sum_{\tau=1}^T a_{T,\tau}$ where $a_{T,\tau}$ is the validation accuracy of task τ after the model finished learning on task T (at test time). The Learning Accuracy is defined as $a_{\tau,\tau}$, this describes how well a model learns a task τ the first time it sees it. The Forgetting Measure is defined as: $F_T = \frac{1}{T-1} \sum_{\tau=1}^{T-1} \max_{t=\{1..T-1\}} (a_{t,\tau} - a_{T,\tau})$. Finally, we define the Forgetting Improvement (FI) simply as the difference between the Forgetting Measure of the single model and the ensemble (or subspace) method as: $FI_T = F_T(\text{single model}) - F_T(\text{ensemble/subspace model})$. Intuitively, the higher this value the less forgetting a method has compared to the single model case.

Algorithms. For this analysis, we compare Vanilla CL (Alg. 2), Ensemble CL (Alg. 3) and Subspace CL (Alg. 4).

3.2 Multiple Models Improve CL Performance

Figs. 4a and 4d show the final average accuracy on both benchmarks. We clearly see the immediate benefits of both the ensemble and subspace methods compared to the single model (black dashed line). For the ensemble method, we also report the performance of each member separately (red dots). Interestingly, "ensembling" them (blue curve) makes a significant improvement compared to every member separately as well as the average of their individual accuracy (orange curve). Note the large benefit for CIFAR-100 dataset. To quantify how much knowledge a model forgets, we use the *forgetting improvement* (FI) previously defined. Fig. 4b and 4e show the FI over the single model and clearly highlight the benefits of having more than one model to mitigate forgetting.

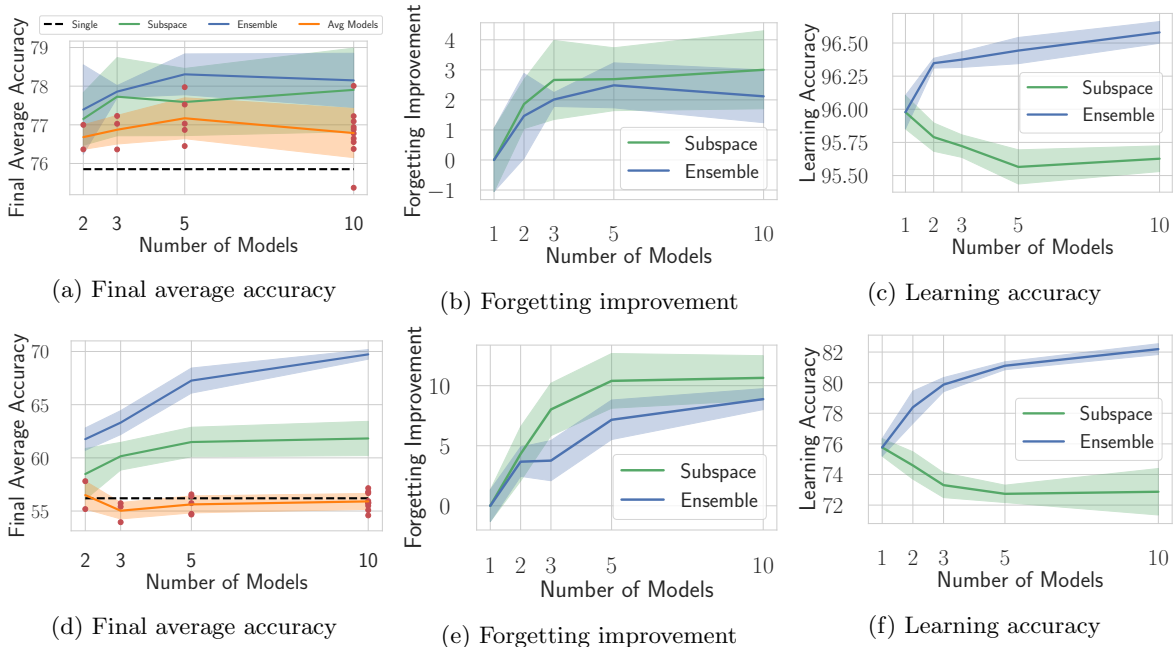


Figure 4: Ablation metrics for Rotated MNIST (first line) and Split CIFAR-100 (second line). Having more models improve the final average accuracy over single model (black dashed line) (**left**). While subspace method mitigates forgetting by tying the weights of its member (**middle**), ensemble method enjoys better learning accuracy as each model moves independently. (**right**).

Given the good performance of ensembles, one may keep adding more models for continued improvement. However, it is either not always helpful (MNIST dataset) or the marginal improvement is not worth the linear compute cost. See Figs 4d and 4e for the relevant results. For the subspace method, increasing the number of models (hence the number of parameters) requires more training epochs to update them. That can explain why after a certain threshold (e.g., $n = 5$ models for Split CIFAR-100), the accuracy and forgetting metrics degrade or plateau given a fixed training budget.

3.3 Training Dynamics of Multiple Models

In this subsection, we focus on the granular dynamics and implications of learning with ensemble vs. learning in subspace. In particular, we investigate how each method differently mitigates CF leading to good performance.

Ensemble methods: diversity is all you need Recall that ensemble methods train independently each member of the ensemble meaning there is no interactions between them during the training. This leads to surprisingly good performance over a single model as shown in the previous section. We believe the power of ensembles and their diversity-enhancing approach (due to random initialization) is very pronounced in the context of continual learning. Figs. 10 and 11 (Appendix) show a boxplot of the diversity in accuracy of the final task for Rotated MNIST and CIFAR-100. First, for each task, a different member has the highest accuracy (diversity of the ensemble). Secondly, the gap between the best member’s individual accuracy (blue) and the ensemble prediction (grey) increases with the number of models (See the last line corresponding to $n = 10$ models).

Subspace methods mitigate CF by learning a low curvature solution While ensemble methods let their member move freely, subspace methods tie each member’s move through a convex combination of their weights. We propose to study the subspace’s property under the loss landscape perspective and the geometry of learning. Keskar et al. (2016); Dinh et al. (2017); Mirzadeh et al. (2020b, 2021a) studied how the curvature of minima in continual learning is linked to generalization and forgetting. They showed that forgetting is bounded by the parameter’s variation between each task and the eigenvalues of the Hessian. Fig. 5 shows that as the number of models increases, the eigenvalues of the subspace solution become smaller. Lower eigenvalues lead to flatter minima and more robustness against forgetting Mirzadeh et al. (2020b). Here we used the Hessian spectrum of the single model as a proxy for the ensemble method. Indeed, the ensemble method corresponds to n single models trained independently with their loss averaged thus the ensemble Hessian spectrum is similar to the single model. Here, for brevity, we provide the Hessian spectrum for the loss of task 1 and postpone further results in the Appendix D.4. Note that for the subspace method, we compute the Hessian spectrum of the midpoint $\omega_{mid} = \frac{1}{n} \sum_{i=1}^n \omega_i$. The flatness of the loss landscape can also be assessed by noise perturbation in the parameter space to observe the variation (decrease) of performance. To that end, we inject multiplicative noise $\mathcal{N}(1, \sigma)$ to the parameters (multiplicative noise scales well to the weights variation magnitude) and compare the performance between ensemble and subspace methods. Fig. 15 shows the ensemble method incurs more performance degradation than the subspace method since it doesn’t benefit from the low loss region (subspace).

Stability-Plasticity dilemma From the stability-plasticity perspective (Mermillod et al., 2013), the subspace method’s solutions are more stable while the ensemble method has more degrees of freedom to change its parameters to learn new tasks, and hence it’s more plastic. To elaborate, look at Figs. 4c and 4f, showing that the ensemble enjoys better learning accuracy. This quantifies how well a model learns a new incoming task. Note that for the ensemble method, as we increase the number of models it reaches as

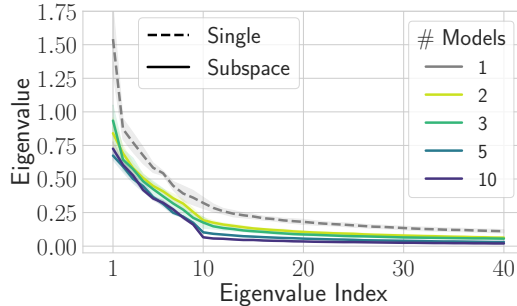


Figure 5: The Hessian spectrum of each model for the loss of task 1 for Rotated MNIST. For subspace methods, the more models the lower the eigenvalues. Lower eigenvalues imply flatter minima which is a proxy to describe how much forgetting will be incurred when learning subsequent tasks.

good forgetting improvement as the subspace method but at the cost of linear growth computational power. On the contrary, the subspace method has less fitting capability since it needs to move each member of the ensemble. It trades off plasticity (learning accuracy) to get more stability (less forgetting).

Overall, each of the above methods uses a different mechanism to mitigate CF (either with diversity enhanced or finding flatter minima by tying each member’s weight together) but in the end ensemble methods get better final accuracy (due to higher learning accuracy). This obviously comes at the cost of linear growth compute cost (See Fig. 3b). For the aforementioned reasons, we focus on the subspace method for the rest of the paper and propose to leverage its property as an efficient alternative approach to ensemble methods. In the next section, we study other properties of neural subspaces in continual learning.

4 Continual Learning with Subspace Models

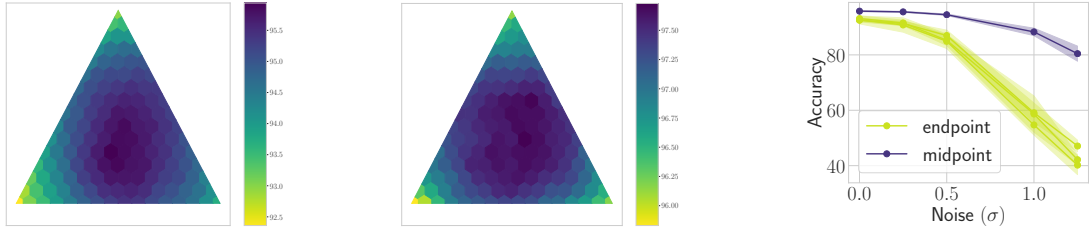
In Sec.3, we saw the benefits of having multiple models in continual learning, especially by learning low-loss regions with subspace methods. This section focuses more deeply on the properties of the subspaces and their implications for continual learning.

To this end, we raise two questions: (1) “What are the interesting properties of the learned subspaces in continual learning?” and (2) “How do subspaces evolve throughout the learning experience?”. In Sec. 4.1, we study the first question and highlight an important property of the subspace method, that is, the center of the subspace contains more accurate and robust solutions. To answer the second question, in Sec. 4.2, we show the limit of the subspace method that can still suffer from the forgetting problem when the number of tasks increases. To address that issue, we finally propose an algorithm (in Sec. 4.3) that exploits the connectivity of the subspaces throughout the continual learning. By connectivity, we mean that there is a path between two solutions along which the loss value and the test error stay low (Draxler et al., 2018; Garipov et al., 2018).

4.1 Subspace midpoint gets the best accuracy

In this section, we further investigate the behavior of the learned subspace ensembles by monitoring the accuracy within the subspace.

To this end, we use Subspace Continual Learning algorithm (Alg. 4) with $n = 3$ models. In Figs. 6a and 6b we show the accuracy across the subspace at the beginning of learning (task 1) and in the middle of learning (task 10), respectively. The plots illustrate that the center (midpoint) has higher learning



(a) Learning accuracy of task 1 (b) Learning accuracy of task 10 (c) Robustness to Gaussian noise around solution's minima.

Figure 6: Rotated MNIST: Learning Accuracy for different tasks inside a subspace region with 3 models. Midpoints (center) show the best performance as opposed to the endpoints (corners) (**left, middle**). Robustness to uniform noise for the case of $n = 3$ models. Midpoint is more robust to weight perturbation than endpoints (**right**)

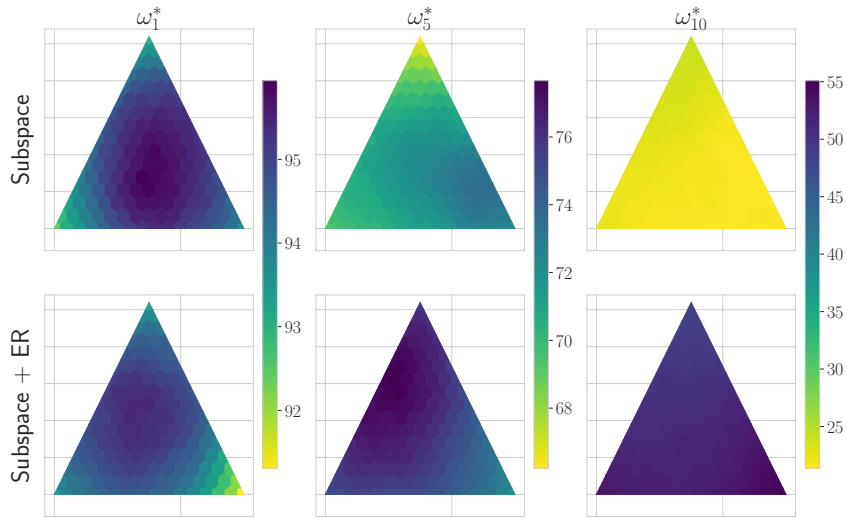


Figure 7: Rotated MNIST: The evolution of accuracy of task 1 throughout the training. Even though the subspace method restricts weight's movement, there is still a noticeable degradation in performance (hence a large amount of forgetting).

accuracy within each region. This also translates into more robustness of the midpoint versus the endpoints (Fig. 6c). In the Appendix (Figs. 13 and 14) we provide a full robustness analysis varying the number of model n in the subspace model. As an interesting observation, the performance of the midpoint gets less affected compared to the endpoints when we increase the number of models. In Sec. 4.3, we use those findings for our proposed algorithm.

4.2 Subspaces still forget

Now, we shift our focus on the evolution of the learned subspaces throughout the continual learning experience. To this end, we compare the subspace method (Alg. 4) with and without Experience Replay, ER (Riemer et al., 2018), (Alg. 5). Fig. 7 shows snapshots of task 1's accuracy across different times of the training (task $\tau = 1, 5, 10$) on Rotated MNIST (20 tasks). We can observe that while adding ER improves the accuracy, over long sequences of tasks, there is still a degradation of performance. For instance, on task 1 Subspace + ER incurs a performance decrease to 55% (last column ω_{10}^*).

To investigate this performance degradation, we employ the recent technique introduced by Mirzadeh

et al. (2021b) where the authors show that the linear mode connectivity can explain the performance gap between continual and multitask solutions. Since the subspace method is inherently motivated by the mode connectivity, we believe investigating the connectivity across subspaces can explain the performance degradation. Hence, we visualize the mode connectivity between successive solutions (represented by midpoints) of task 1 and task 2, evaluated on the loss of task 1. In Fig. 8 we can see that the midpoints of subsequent subspaces’ solutions are not *linearly connected* meaning the linear interpolated weights between these two solutions does not stay in a low-loss region (Mirzadeh et al., 2021b). Fig 17 in Appendix provides more detailed analysis and metrics (including accuracy) with the same conclusion.

Thus far, we have investigated the properties of the subspaces and their evolution throughout the learning experience. We have observed in Sec. 3 the subspace method yields more accurate and robust solutions for continual learning, and the center of the subspace contains more robust solutions. However, by tracking the evolution of the subspace, we have also observed a performance degradation, which can be explained by the lack of connectivity between solutions. These results motivate our next section, where we design an algorithm that takes these findings into action.

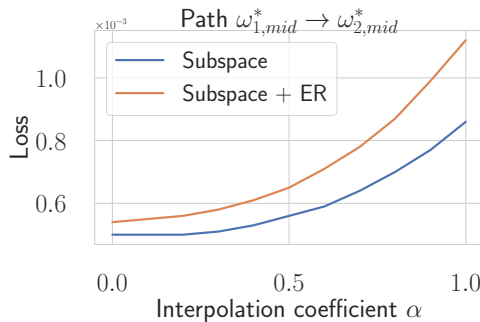


Figure 8: Rotated MNIST: The sequential subspace solutions are not linearly connected.

4.3 Improving Subspace Learning with Connectivity

In this section, based on our analysis in Sec. 4.2, we propose Subspace-Connectivity . Our algorithm is based on the subspace method introduced in Sec. 3 with the following modifications. First, we use the midpoint as a proxy for the subspace solution of the learned task (Sec. 4.1), and second, we use experience replay for connecting the subspaces throughout the learning (Sec. 4.2). Subspace-Connectivity (*c.f.* Alg. 1) has two main steps and details on the implementations can be found in Appendix E.1.

Learning a subspace solution for the incoming task : The first step consists in learning a subspace solution by fine-tuning on task τ leading to the solution $\widehat{W}_\tau = \{\widehat{w}_{\tau,i}\}_{i=1}^n$ obtained by optimizing:

$$\{\widehat{w}_{\tau,i}\}_{i=1}^n = \operatorname{argmin}_W \mathbb{E}_{\alpha \sim \mathcal{U}[\Delta^n]} [\mathcal{L}_\tau(W^T \alpha)]^4. \quad (4.1)$$

At the end of this step, we save in a buffer memory \mathcal{B} , m_B samples per class per task that will be used to connect linearly two subspace’s solutions.

Connecting subsequent solutions together: This step aims at connecting subspaces from prior task’s solutions together as in MC-SGD (Mirzadeh et al., 2021b). First, we use the midpoint of subspace τ denoted $\widehat{\omega}_{\tau,mid}^*$ as its proxy since it gives the best performance (Sec. 4.1). We then connect $\widehat{\omega}_{\tau,mid}^*$ and previous tasks midpoint solution $\omega_{\tau-1,mid}^*$ via a low loss path. The loss over the connecting path acts as a penalty or regularizer term.

⁴We also tried the cosine regularization as in (Wortsman et al., 2020) without much difference in performance.

Algorithm 1 Subspace-Connectivity CL

Input : A task sequence $\mathcal{T}_1, \mathcal{T}_2, \dots, \mathcal{T}_T$, number of models n , buffer \mathcal{B} and memory size $m_{\mathcal{B}}$

1. Initialize set of weights $S^n = \{\omega_{0,i}\}_{i=1}^n$, buffer $\mathcal{B} \leftarrow \{\}$

2. **for** tasks $\tau = 1, 2, 3, \dots, T$ **do**

 Get $\{\hat{\omega}_{\tau,i}^*\}_{i=1}^n$ with Eq 4.1

 //Learn subspaces solution for task τ

for $(x, y) \in \mathcal{T}_\tau$ **do**

$\mathcal{B} \leftarrow \mathcal{B} \cup \{x, y\}$

end for

 Get $\{\omega_{\tau,i}^*\}_{i=1}^n$ with Eq 4.2 using samples from \mathcal{B}

 //Connect previous solution' subspaces

end for

Output : $\{\omega_{T,i}^*\}_{i=1}^n$

This is done by optimizing the following loss with saved elements from the buffer:

$$\{\omega_{\tau,i}^*\}_{i=1}^n = \underset{W}{\operatorname{argmin}} \mathbb{E}_{\alpha \sim \mathcal{U}(\Delta^{n+1})} \left[\sum_{j=1}^{\tau-1} \mathcal{L}_j(W^T \alpha^n + \alpha_{n+1} \omega_{\tau-1, \text{mid}}^*) \right] + \mathcal{L}_\tau(W^T \alpha^n + \alpha_{n+1} \hat{\omega}_{\tau, \text{mid}}) \quad (4.2)$$

where $\alpha = (\underbrace{\alpha_1, \dots, \alpha_n}_{\alpha^n \in \mathbb{R}^n}, \alpha_{n+1}) \in \mathbb{R}^{n+1}$ and \mathcal{L}_j corresponds to the loss of task j (using element of task j from the buffer). The rationale behind this loss function is to create a linear path of low-loss between two subsequent solutions $\omega_{\tau-1, \text{mid}}^*$ and $\omega_{\tau, \text{mid}}^*$.

A few remarks worth noting here. Intuitively speaking, the subspace method ties the models for a single task, while the mode connectivity regularization ties the subspaces together. Note that the original subspace method is only developed for single-task settings, which, although improves the performance, still does not have any mechanism to learn from a sequence of tasks. As a result, we can see that there is a noticeable forgetting as the number of tasks increases (see Figs. 7 and 8). Hence, we use the mode connectivity regularization to connect the solutions, which are shown to be an important property of multitask solutions Mirzadeh et al. (2021b). Fig. 19 and 17 show that our regularization term allows a quasi non decreasing linear path between subsequent solutions (denoted "Ours"). Note also the gradients of this regularization are passed via midpoints indirectly. If the endpoints are not properly located, their midpoints impose a penalty which will be backpropagated to the endpoints for further adjustment facilitated via coefficients α .

5 Experiments and Results

In this section, we compare Subspace-Connectivity with several state-of-the-art algorithms. Due to space limitations, we postpone several experiments and results to the Appendix. In Appendix F.2, we study the impact of the number of models being used on the performance. Table 3 provides a performance comparison of Subspace-Connectivity when we vary the number of models. Moreover, Tables 4 and 5 provide a comparison of performance and computation cost against scaled version and ensemble methods, while Table 6 provides a comparison between different strategies of ensemble methods (bagging versus training independently). Finally, Appendix D.6.1 provides further results on the subspace connectivity, and in Fig. 19, we show that the solutions obtained by Subspace-Connectivity are linearly connected as discussed in Sec. 4.3.

5.1 Comparison Against Baseline Methods

Performance. Tables 1 and 8 summarize the average accuracy and forgetting for each algorithm. For our method (Subspace-Connectivity), we report the results of the midpoint since it yields the best accuracy as we have discussed in Sec. 4.1. Moreover, Fig. 20 (Appendix) shows the evolution of average accuracy for each method on each benchmark. Overall, Subspace-Connectivity is improving over MC-SGD (of 3% on average over the four benchmarks).

Efficiency. We recall that an important objective of this work is the performance and computational costs in continual learning. To this end, we compare the accuracy for different levels of computation in Figs. 9 and 21. From these results, we can draw several conclusions. First, as we have discussed in Sec. 3, the ensemble can outperform a larger single model (with an augmented number of parameters) with the same amount of computation. Finally, and more importantly, Subspace-Connectivity can match or exceed the accuracy of both ensembles and large single models with a much smaller amount of computation.

Overall, our proposed method Subspace-Connectivity performs at least on par with ensemble methods (if not better for some datasets) but enjoys a drastic computational cost reduction.

Table 1: Comparison between the proposed method (Subspace-Connectivity) and other baselines on 5 random seeds (\pm std).

Method	Permuted MNIST		Rotated MNIST		Split CIFAR-100	
	Accuracy \uparrow	Forgetting \downarrow	Accuracy \uparrow	Forgetting \downarrow	Accuracy \uparrow	Forgetting \downarrow
Naive SGD	44.4 (± 2.46)	0.53 (± 0.03)	46.3 (± 1.37)	0.52 (± 0.01)	40.4 (± 2.83)	0.31 (± 0.02)
EWC (Kirkpatrick et al., 2017)	70.7 (± 1.74)	0.23 (± 0.01)	48.5 (± 1.24)	0.48 (± 0.01)	42.7 (± 1.89)	0.28 (± 0.03)
A-GEM (Chaudhry et al., 2019a)	65.7 (± 0.51)	0.29 (± 0.01)	55.3 (± 1.47)	0.42 (± 0.01)	50.7 (± 2.32)	0.19 (± 0.04)
ER-Reservoir (Chaudhry et al., 2019b)	72.4 (± 0.42)	0.16 (± 0.01)	69.2 (± 1.10)	0.21 (± 0.01)	46.9 (± 0.76)	0.21 (± 0.03)
Stable SGD (Mirzadeh et al., 2020b)	80.1 (± 0.51)	0.09 (± 0.01)	70.8 (± 0.78)	0.10 (± 0.02)	56.9 (± 1.52)	0.11 (± 0.01)
MC-SGD (Mirzadeh et al., 2021b)	82.9 (± 0.40)	0.10 (± 0.01)	81.9 (± 0.46)	0.08 (± 0.01)	58.2 (± 0.91)	0.08 (± 0.01)
Subspace-Connectivity (ours)	87.8 (± 0.53)	0.06 (± 0.01)	86.7 (± 0.67)	0.07 (± 0.01)	61.7 (± 0.80)	0.05 (± 0.01)
Multitask Learning	89.5 (± 0.21)	0.0	89.8 (± 0.37)	0.0	66.8 (± 1.42)	0.0

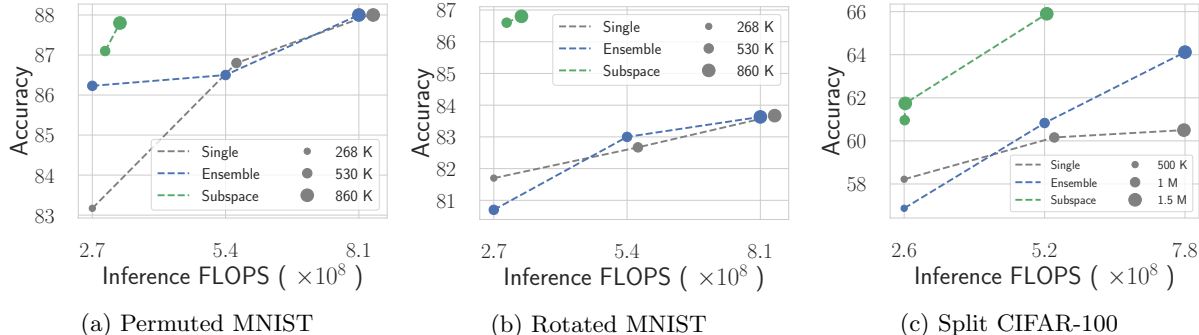


Figure 9: Performance of MC-SGD (Single), Ensemble MC-SGD (Ensemble) and Subspace-Connectivity (Subspace) with respect to the inference cost (FLOPS) and number of parameters/models n (circles).

6 Related Work

The methodology to tackle catastrophic forgetting for continual learning has been extensively populated with three main groups.

Continual learning. Among pioneer methods to alleviate the catastrophic forgetting, we can name *regularization-based* methods that limit the drift in important parameters of features of past tasks (Kirkpatrick et al., 2017; Zenke et al., 2017; Nguyen et al., 2017; Yin et al., 2020). For instance, EWC Kirkpatrick

et al. (2017) uses the Fisher information to identify the important parameters. A major drawback of the regularization methods is that they often need multiple passes over data to perform well Chaudhry et al. (2019a) and when the number of tasks is large, they suffer more from the feature drift (Titsias et al., 2020).

The second group of methods in continual learning is the *memory-based* methods that keep a small episodic memory of data from past tasks to either replay those examples Chaudhry et al. (2019b); Rebuffi et al. (2017); Riemer et al. (2018); Lesort (2020) or use them for improving the optimization procedure such as projection methods Farajtabar et al. (2020); Bennani et al. (2020); Saha et al. (2021), or train a generative model to serve that purpose (Shin et al., 2017; Kirichenko et al., 2021). A-GEM Chaudhry et al. (2019a) is a notable example of these methods that use gradients of past tasks to modify the gradients of the new task and alleviate the forgetting.

Finally, *parameter isolation* methods focus on the neural network modules that can be either be expanded for each new task Aljundi et al. (2017) or a sub-network will be allocated for each task Wortsman et al. (2020); Fernando et al. (2017), or create implicit gateways for different tasks (Mirzadeh et al., 2020a). However, the expansion-based methods’ memory and compute requirement grows as the number of tasks grows. In addition, these methods rely on the task identifiers for selecting the appropriate module for prediction and often cannot operate without this information.

Perhaps our work is mainly related to regularization- and memory-based methods. Our proposed algorithm maintains a memory of past data for regularization purposes (i.e., encouraging the connectivity between subspaces across tasks).

Mode connectivity. (Draxler et al., 2018; Garipov et al., 2018) studied the loss landscape and existence of connectivity of neural networks solutions. They discovered the existence of pathways/curves of non-increasing loss between solutions optima. In the context of continual learning, (Mirzadeh et al., 2021b) have recently shown that multitask and continual minima are connected via low-loss paths and leveraged this property to connect tasks’ minima in continual learning and proposed the MC-SGD algorithm, which encourages the linear connectivity between tasks’ minima via path regularization. While our work is inspired by their findings, we note that MC-SGD is developed with a single model continual learning in mind, while we extend their work for the continual learning setup with multiple models.

Neural network subspaces. (Wortsman et al., 2021; Benton et al., 2021) recently proposed to connect solution of an ensemble of models through a region in the weight space known as *subspace*. That region is a low loss surface and shown to outperform the solution of ensemble models. (Gaya et al., 2021) learned a subspace of policies in the reinforcement learning context for fast adaptation. While our work is directly motivated by the subspace literature, we note that these methods have been studied in single-task settings. In contrast, our work extends them for continual learning with a sequence of tasks rather than a single task.

7 Conclusion

While the focus of continual learning literature is mainly on studying the problem with a single model, in this work, we extended it to the multiple models’ case. More specifically, we are the first to investigate the diversity enhanced power of ensemble methods in the continual learning context. This leads to better performance than subspace, but at the cost of high computational cost growth.

To overcome this challenge, we have studied the neural network subspaces for efficient ensembling in continual learning, and inspired by the recent advances in the mode connectivity literature, we have focused on the evolution of these subspaces in continual learning. Motivated by the limits of the subspaces, we have developed Subspace-Connectivity that outperforms state-of-the-art algorithms in various benchmarks

yet enjoys being as computationally cheap as a single model training.

We believe our work can be a stepping-stone for several future works, such as further studying the interactions between multiple models in continual learning or exploiting the subspace’s region property to improve the continual learning performance.

Acknowledgements

We would like to thank (alphabetical order) Mehdi Bennani, Lucas Caccia, Ludovic Denoyer, Timothée Lesort, Yee Why Teh, Maxime Wabartha, Dong Yin for useful discussions and feedbacks throughout the work. We acknowledge research grants from Canadian Institute for Advanced Research (CIFAR) and Natural Sciences and Engineering Research Council of Canada (NSERC). TD holds a fellowship funded by IVADO.

References

- Aljundi, R., Chakravarty, P., and Tuytelaars, T. (2017). Expert gate: Lifelong learning with a network of experts. In *2017 IEEE Conference on Computer Vision and Pattern Recognition (CVPR)*, pages 7120–7129.
- Bennani, M. A., Doan, T., and Sugiyama, M. (2020). Generalisation guarantees for continual learning with orthogonal gradient descent. *arXiv preprint arXiv:2006.11942*.
- Benton, G. W., Maddox, W., Lotfi, S., and Wilson, A. G. (2021). Loss surface simplexes for mode connecting volumes and fast ensembling. In Meila, M. and Zhang, T., editors, *Proceedings of the 38th International Conference on Machine Learning, ICML 2021, 18-24 July 2021, Virtual Event*, volume 139 of *Proceedings of Machine Learning Research*, pages 769–779. PMLR.
- Breiman, L. (1996). Bagging predictors. *Machine learning*, 24(2):123–140.
- Caccia, L., Xu, J., Ott, M., Ranzato, M., and Denoyer, L. (2021). On anytime learning at macroscale. *arXiv preprint arXiv:2106.09563*.
- Chaudhry, A., Ranzato, M., Rohrbach, M., and Elhoseiny, M. (2019a). Efficient lifelong learning with a-GEM. In *International Conference on Learning Representations*.
- Chaudhry, A., Rohrbach, M., Elhoseiny, M., Ajanthan, T., Dokania, P. K., Torr, P. H., and Ranzato, M. (2019b). On tiny episodic memories in continual learning. *arXiv preprint arXiv:1902.10486*.
- Dietterich, T. G. (2000). Ensemble methods in machine learning. In *International workshop on multiple classifier systems*, pages 1–15. Springer.
- Dinh, L., Pascanu, R., Bengio, S., and Bengio, Y. (2017). Sharp minima can generalize for deep nets. In *International Conference on Machine Learning*, pages 1019–1028. PMLR.
- Doan, T., Bennani, M. A., Mazouze, B., Rabusseau, G., and Alquier, P. (2021). A theoretical analysis of catastrophic forgetting through the ntk overlap matrix. In *International Conference on Artificial Intelligence and Statistics*, pages 1072–1080. PMLR.
- Draxler, F., Veschgini, K., Salmhofer, M., and Hamprecht, F. (2018). Essentially no barriers in neural network energy landscape. In *ICML 2018: Thirty-fifth International Conference on Machine Learning*, pages 1308–1317.
- Farajtabar, M., Azizan, N., Mott, A., and Li, A. (2020). Orthogonal gradient descent for continual learning. In *International Conference on Artificial Intelligence and Statistics*, pages 3762–3773. PMLR.
- Fernando, C., Banarse, D., Blundell, C., Zwols, Y., Ha, D., Rusu, A. A., Pritzel, A., and Wierstra, D. (2017). Pathnet: Evolution channels gradient descent in super neural networks. *arXiv preprint arXiv:1701.08734*.
- Fort, S., Hu, H., and Lakshminarayanan, B. (2019). Deep ensembles: A loss landscape perspective. *arXiv preprint arXiv:1912.02757*.
- Garipov, T., Izmailov, P., Podoprikin, D., Vetrov, D., and Wilson, A. (2018). Loss surfaces, mode connectivity, and fast ensembling of dnns. In *NeurIPS 2018: The 32nd Annual Conference on Neural Information Processing Systems*, pages 8789–8798.
- Gaya, J.-B., Soulier, L., and Denoyer, L. (2021). Learning a subspace of policies for online adaptation in reinforcement learning. *arXiv preprint arXiv:2110.05169*.
- Goodfellow, I. J., Mirza, M., Da, X., Courville, A. C., and Bengio, Y. (2014a). An empirical investigation of catastrophic forgetting in gradient-based neural networks. *CoRR*, abs/1312.6211.

- Goodfellow, I. J., Shlens, J., and Szegedy, C. (2014b). Explaining and harnessing adversarial examples. *arXiv preprint arXiv:1412.6572*.
- Havasi, M., Jenatton, R., Fort, S., Liu, J. Z., Snoek, J., Lakshminarayanan, B., Dai, A. M., and Tran, D. (2020). Training independent subnetworks for robust prediction. *arXiv preprint arXiv:2010.06610*.
- Huang, G., Li, Y., Pleiss, G., Liu, Z., Hopcroft, J. E., and Weinberger, K. Q. (2017). Snapshot ensembles: Train 1, get m for free. *arXiv preprint arXiv:1704.00109*.
- Keskar, N. S., Mudigere, D., Nocedal, J., Smelyanskiy, M., and Tang, P. T. P. (2016). On large-batch training for deep learning: Generalization gap and sharp minima. *arXiv preprint arXiv:1609.04836*.
- Kirichenko, P., Farajtabar, M., Rao, D., Lakshminarayanan, B., Levine, N., Li, A., Hu, H., Wilson, A. G., and Pascanu, R. (2021). Task-agnostic continual learning with hybrid probabilistic models. In *ICML Workshop on Invertible Neural Networks, Normalizing Flows, and Explicit Likelihood Models*.
- Kirkpatrick, J., Pascanu, R., Rabinowitz, N., Veness, J., Desjardins, G., Rusu, A. A., Milan, K., Quan, J., Ramalho, T., Grabska-Barwinska, A., and et al. (2017). Overcoming catastrophic forgetting in neural networks. *Proceedings of the National Academy of Sciences*, 114(13):3521–3526.
- Krizhevsky, A. et al. (2009). Learning multiple layers of features from tiny images. *CoRR*.
- Lakshminarayanan, B., Pritzel, A., and Blundell, C. (2017). Simple and scalable predictive uncertainty estimation using deep ensembles. *Advances in Neural Information Processing Systems*, 30.
- Lesort, T. (2020). Continual learning: Tackling catastrophic forgetting in deep neural networks with replay processes. *arXiv preprint arXiv:2007.00487*.
- Lesort, T., George, T., and Rish, I. (2021). Continual learning in deep networks: an analysis of the last layer. *arXiv preprint arXiv:2106.01834*.
- Manolis Savva*, Abhishek Kadian*, Oleksandr Maksymets*, Zhao, Y., Wijmans, E., Jain, B., Straub, J., Liu, J., Koltun, V., Malik, J., Parikh, D., and Batra, D. (2019). Habitat: A Platform for Embodied AI Research. In *Proceedings of the IEEE/CVF International Conference on Computer Vision (ICCV)*.
- McCloskey, M. and Cohen, N. J. (1989). Catastrophic interference in connectionist networks: The sequential learning problem. In *Psychology of learning and motivation*, volume 24, pages 109–165. Elsevier.
- Mermillod, M., Bugaiska, A., and Bonin, P. (2013). The stability-plasticity dilemma: Investigating the continuum from catastrophic forgetting to age-limited learning effects. *Frontiers in psychology*, 4:504.
- Mirzadeh, S. I., Chaudhry, A., Hu, H., Pascanu, R., Gorur, D., and Farajtabar, M. (2021a). Wide neural networks forget less catastrophically. *ArXiv*, abs/2110.11526.
- Mirzadeh, S. I., Farajtabar, M., and Ghasemzadeh, H. (2020a). Dropout as an implicit gating mechanism for continual learning. In *Proceedings of the IEEE/CVF Conference on Computer Vision and Pattern Recognition Workshops*, pages 232–233.
- Mirzadeh, S. I., Farajtabar, M., Gorur, D., Pascanu, R., and Ghasemzadeh, H. (2021b). Linear mode connectivity in multitask and continual learning. In *International Conference on Learning Representations*.
- Mirzadeh, S. I., Farajtabar, M., Pascanu, R., and Ghasemzadeh, H. (2020b). Understanding the role of training regimes in continual learning. In Larochelle, H., Ranzato, M., Hadsell, R., Balcan, M. F., and Lin, H., editors, *Advances in Neural Information Processing Systems*, volume 33, pages 7308–7320.
- Nguyen, C. V., Li, Y., Bui, T. D., and Turner, R. E. (2017). Variational continual learning. In *International Conference on Learning Representations*.

- Rebuffi, S.-A., Kolesnikov, A., Sperl, G., and Lampert, C. H. (2017). icarl: Incremental classifier and representation learning. In *2017 IEEE Conference on Computer Vision and Pattern Recognition (CVPR)*, volume 2017, pages 5533–5542.
- Riemer, M., Cases, I., Ajemian, R., Liu, M., Rish, I., Tu, Y., and Tesauro, G. (2018). Learning to learn without forgetting by maximizing transfer and minimizing interference. In *International Conference on Learning Representations*.
- Russakovsky, O., Deng, J., Su, H., Krause, J., Satheesh, S., Ma, S., Huang, Z., Karpathy, A., Khosla, A., Bernstein, M., Berg, A. C., and Fei-Fei, L. (2015). ImageNet Large Scale Visual Recognition Challenge. *International Journal of Computer Vision (IJCV)*, 115(3):211–252.
- Saha, G., Garg, I., and Roy, K. (2021). Gradient projection memory for continual learning. In *International Conference on Learning Representations*.
- Shin, H., Lee, J. K., Kim, J., and Kim, J. (2017). Continual learning with deep generative replay. In *Advances in Neural Information Processing Systems*, pages 2990–2999.
- Szot, A., Clegg, A., Undersander, E., Wijmans, E., Zhao, Y., Turner, J., Maestre, N., Mukadam, M., Chaplot, D., Maksymets, O., Gokaslan, A., Vondrus, V., Dharur, S., Meier, F., Galuba, W., Chang, A., Kira, Z., Koltun, V., Malik, J., Savva, M., and Batra, D. (2021). Habitat 2.0: Training home assistants to rearrange their habitat. *arXiv preprint arXiv:2106.14405*.
- Thrun, S. (1994). A lifelong learning perspective for mobile robot control. In *Proceedings of IEEE/RSJ International Conference on Intelligent Robots and Systems (IROS'94)*, volume 1, pages 23–30 vol.1.
- Titsias, M. K., Schwarz, J., de G. Matthews, A. G., Pascanu, R., and Teh, Y. W. (2020). Functional regularisation for continual learning with gaussian processes. In *ICLR 2020 : Eighth International Conference on Learning Representations*.
- Wen, Y., Tran, D., and Ba, J. (2020). Batchensemble: an alternative approach to efficient ensemble and lifelong learning. In *International Conference on Learning Representations*.
- Wortsman, M., Horton, M., Guestrin, C., Farhadi, A., and Rastegari, M. (2021). Learning neural network subspaces.
- Wortsman, M., Ramanujan, V., Liu, R., Kembhavi, A., Rastegari, M., Yosinski, J., and Farhadi, A. (2020). Supermasks in superposition. In *Advances in Neural Information Processing Systems*, volume 33, pages 15173–15184.
- Yin, D., Farajtabar, M., Li, A., Levine, N., and Mott, A. (2020). Optimization and generalization of regularization-based continual learning: a loss approximation viewpoint. *arXiv preprint arXiv:2006.10974*.
- Zenke, F., Poole, B., and Ganguli, S. (2017). Continual learning through synaptic intelligence.

A Appendix

The appendix is organized as follows:

- Appendix B compares the computational cost implications of ensemble and subspace models.
- Appendix C provides pseudo-code of algorithms used in our ablations analysis and final experiments section.
- Appendix D shows additional ablation analysis that highlights benefits and drawbacks of ensemble and subspace methods (Section 3).
- Appendix D.6 provides an in-depth investigation of the properties of subspace learning throughout the training.
- Appendix E details the experimental setup of our final results on 20 tasks for MNIST and CIFAR-100 dataset (Section F)
- Appendix F.2 provides performance and computational cost of Subspace-Connectivity against ensemble methods and larger models

B Computational cost implications for ensemble and subspace methods

This section discusses the implication cost of ensemble and subspace methods.

For the ensemble methods, since each model is trained independently on the same dataset, the cost is n times higher (n times more forward and backward passes).

Compared to the single model, the subspace method contains one additional operation for the inference and backpropagation operation. Before the inference, a convex combination of the weights is sampled:

$\bar{\omega} = \sum_{i=1}^n \alpha_i \omega_i$, $\alpha \sim \mathcal{U}(\Delta^n)$ (weights mixing). For the backpropagation, only one backward pass is needed ($\frac{\partial \mathcal{L}}{\partial \bar{\omega}}$) before assigning the new weights $\omega_i = \omega_i - l_r \alpha_i \frac{\partial \mathcal{L}}{\partial \bar{\omega}}$, $\forall i = 1 \dots n$, l_r being the learning rate.

Overall, the subspace method has only two supplementary addition operations as an overhead cost compared to the single model which is much cheaper than the $n - 1$ additional forward and backward pass of the ensemble methods. This makes the subspace method more efficient.

Method	forward pass	backward pass
Single model	1 inference pass ($f(x, \omega)$)	1 backpropagation pass ($\frac{\partial \mathcal{L}}{\partial \omega}$)
Ensemble	n inference passes ($f(x, \omega_i), \forall i = 1 \dots n$)	n backpropagations passes ($\frac{\partial \mathcal{L}}{\partial \omega_i}, \forall i = 1 \dots n$)
Subspace	$\bar{\omega} = \sum_{i=1}^n \alpha_i \omega_i$ 1 inference pass ($f(x, \bar{\omega})$)	1 backpropagation pass ($\frac{\partial \mathcal{L}}{\partial \bar{\omega}}$) $\omega_i \leftarrow \omega_i - l_r \alpha_i \frac{\partial \mathcal{L}}{\partial \bar{\omega}}, \forall i = 1 \dots n$

Table 2: Computational cost comparison between different methods. In red are the additional operations compared to the single model. While ensemble methods have $(n - 1)$ additional backward passes (backward pass), subspace methods only incur addition operations as an overhead cost which are much cheaper.

C Algorithms pseudo-code

Algorithm 2 Vanilla Continual Learning (Single Model)

Input : A task sequence $\mathcal{T}_1, \mathcal{T}_2, \dots, \mathcal{T}_T$, loss function \mathcal{L}
Initialize weights ω_0^*
for tasks $\tau = 1, 2, 3, \dots, T$ **do**
 for $(x, y) \in \mathcal{T}_\tau$ **do**
 Get $f_{\omega_{\tau-1}}(x)$
 Optimize $\mathcal{L}(f_{\omega_{\tau-1}}(x), y)$ //Fine-tune on task τ
 end for
 Return ω_τ^*
end for
Output : ω_T^*

Algorithm 3 Ensemble Continual Learning

Input : A task sequence $\mathcal{T}_1, \mathcal{T}_2, \dots, \mathcal{T}_T$, loss function \mathcal{L} , number of models n
Initialize set of weights $\{\omega_{i,0}\}_{i=1}^n$
for tasks $\tau = 1, 2, 3, \dots, T$ **do**
 for $(x, y) \in \mathcal{T}_\tau$ **do**
 Get $f_{\omega_{i,\tau-1}}(x), \forall i = 1 \dots n$
 Optimize $\frac{1}{n} \sum_{i=1}^n \mathcal{L}(f_{\omega_{i,\tau-1}}(x), y)$ //Update each model independently: requires n backward passes
 end for
 Return $\{\omega_{i,\tau}^*\}_{i=1}^n$
end for
Output : $\{\omega_{i,T}^*\}_{i=1}^n$

Algorithm 4 Subspace Continual Learning

Input : A task sequence $\mathcal{T}_1, \mathcal{T}_2, \dots, \mathcal{T}_T$, loss function \mathcal{L} , number of models n
Initialize set of weights $\{\omega_{i,0}\}_{i=1}^n$
for tasks $\tau = 1, 2, 3, \dots, T$ **do**
 for $(x, y) \in \mathcal{T}_\tau$ **do**
 $\alpha \sim \mathcal{U}(\Delta^n), \bar{\omega}_{\tau-1} = \sum_i \alpha_i \omega_{i,\tau-1}$ //Sample uniformly convex combination of weights
 Get $f_{\bar{\omega}_{\tau-1}}(x)$
 Optimize $\mathcal{L}(f_{\bar{\omega}_{\tau-1}}(x), y)$
 end for
 Return $\{\omega_{i,\tau}^*\}_{i=1}^n$
end for
Output : $\{\omega_{i,T}^*\}_{i=1}^n$

Algorithm 5 Subspace + Experience Replay (ER)

Input : A task sequence $\mathcal{T}_1, \mathcal{T}_2, \dots, \mathcal{T}_T$, loss function \mathcal{L} , number of models n , replay buffer \mathcal{B} , $m_{\mathcal{B}}$ memory size per task

Initialize set of weights $\{\omega_{i,0}\}_{i=1}^n$

```
for tasks  $\tau = 1, 2, 3, \dots, T$  do
  for  $(x, y) \in \mathcal{T}_\tau$  do
     $\alpha \sim \mathcal{U}(\Delta^n)$ ,  $\bar{\omega}_{\tau-1} = \sum_i \alpha_i \omega_{i,\tau-1}$  //Sample uniformly convex combination of weights
     $(x', y') \sim \mathcal{B}$  //Samples elements from the buffer
     $x \leftarrow \text{Concat}(x, x')$ 
     $y \leftarrow \text{Concat}(y, y')$ 
    Get  $f_{\bar{\omega}_{\tau-1}}(x)$ 
    Optimize  $\mathcal{L}(f_{\bar{\omega}_{\tau-1}}(x), y)$ 
  end for
  Return  $\{\omega_{i,\tau}^*\}_{i=1}^n$ 
  for  $(x, y) \in \mathcal{T}_\tau$  do
     $\mathcal{B} \leftarrow \mathcal{B} \cup \{x, y\}$  //Store  $m_{\mathcal{B}}$  elements per class per task in the buffer
  end for
end for
Output :  $\{\omega_{i,T}^*\}_{i=1}^n$ 
```

Algorithm 6 Subspace-Connectivity CL

Input : A task sequence $\mathcal{T}_1, \mathcal{T}_2, \dots, \mathcal{T}_T$, number of models n , buffer \mathcal{B} and memory size $m_{\mathcal{B}}$

1. Initialize set of weights $S^n = \{\omega_{0,i}\}_{i=1}^n$, buffer $\mathcal{B} \leftarrow \{\}$

2. for tasks $\tau = 1, 2, 3, \dots, T$ do

Get $\{\hat{\omega}_{\tau,i}^*\}_{i=1}^n$ with Eq 4.1

//Learn subspaces solution for task τ

for $(x, y) \in \mathcal{T}_\tau$ do

| $\mathcal{B} \leftarrow \mathcal{B} \cup \{x, y\}$

end for

Get $\{\omega_{\tau,i}^*\}_{i=1}^n$ with Eq 4.2 using samples from \mathcal{B}

//Connect previous solution' subspaces

end for

Output : $\{\omega_{T,i}^*\}_{i=1}^n$

D Setup of ablation and additional results

D.1 Experimental parameters

For the ablation of Section 3, we train on 5 tasks for Rotated MNIST and Split CIFAR-100. The details of the setup are the following:

Rotated MNIST : The incremental angle is 22.5° for a total of 90° . This made the benchmark more challenging as done in (Mirzadeh et al., 2020b) with one training epoch per task.

Split CIFAR-100 : We use the 25 first tasks of CIFAR-100 and train for 5 epochs per task to highlight the properties of ensemble methods.

The hyperparameters for each baseline are the following:

Naive SGD and Ensemble Continual Learning

- learning rate: [0.2, 0.15, **0.1** (MNIST), **0.05** (CIFAR-100), 0.01]
- learning rate decay: [1.0 (CIFAR-100)⁵, 0.95, 0.9, 0.5 (MNIST)]
- batch size: 10

Subspace Continual Learning

- standardized learning rate⁶: [0.2, **0.15** (CIFAR-100), **0.1** (MNIST)]
- learning rate decay: [1.0 (CIFAR-100), 0.95, 0.9, 0.5 (MNIST)]
- batch size: 10

An other important aspect of subspace methods are how close each model is initialized. The further away from each other they are, the more iteration will be needed to update the whole volume. To control this volume, we initialize each model’s weight with respect to the first one as: $\omega_i = \omega_1 * \mathcal{N}(1, \sigma_{init})$, $\forall i = 1 \dots n$, ω_1 being the initialized weight of the first model. The variance σ_{init} controls this volume. For MNIST, we use $\sigma_{init} = 1.0$ ($n = 2, 3$) and $\sigma_{init} = 1.5$ ($n = 5, 10$), for CIFAR-100 we use $\sigma_{init} = 0.1$ ($n = 2, 3, 5, 10$).

D.2 Metrics

To quantify the properties of ensemble and subspace methods, we have used the following metrics:

Learning Accuracy $LA_T = \frac{1}{T} \sum_{\tau=1}^T a_{\tau, \tau}$, where $a_{\tau, \tau}$ represents the accuracy on task τ after learning on task τ the first time, **Forgetting** $F_T = \frac{1}{T-1} \sum_{\tau=1}^{T-1} \max_{t=\{1..T-1\}} (a_{t, \tau} - a_{T, \tau})$ and **Forgetting Improvement** $FI_T = F_T(\text{single model}) - F_T(\text{ensemble/subspace model})$

⁵A value of 1 means no decay has been applied to the learning rate

⁶This is an average learning rate per model, i.e we use a learning rate of 0.3 when using $n = 3$ models for MNIST

D.3 Diversity of the ensemble methods

To measure the diversity of each member in the ensemble method (Ensemble Continual Learning Alg. 3), we show the boxplot of the final average accuracy for each member of the ensemble (line) on each task (column) in Figure 10. The x-axis represents each individual in the ensemble while the last index represents the final prediction of the ensemble (noted "Avg"). As we increase the number of models, the gap between the highest accuracy of each individual and the final prediction increases (For instance, compare gap between blue and gray boxplot for the 3rd column). The diversity in each model (initialized differently) might explain good performance of ensemble methods.

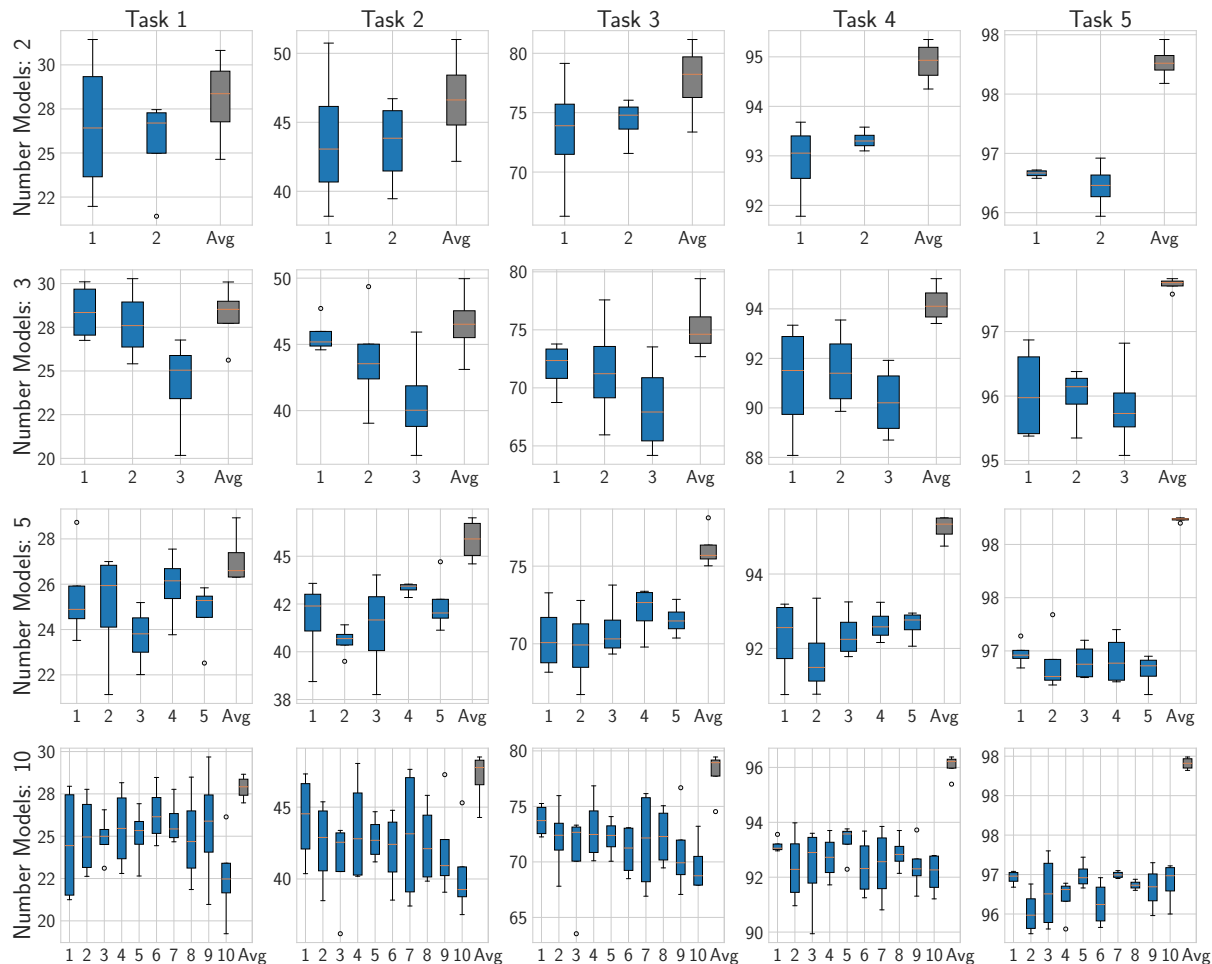


Figure 10: Final accuracy for each model of the ensemble (blue) and the final ensemble prediction (gray) for each task for Rotated MNIST. The final ensemble prediction accuracy is almost always higher than the best accuracy of the best model. As we increase the number of models, we can see a diversity in the prediction of each model, each of them seems to specialize naturally in diverse tasks (look at $n = 5, 10$). This might contribute to the good performance of the ensemble method.

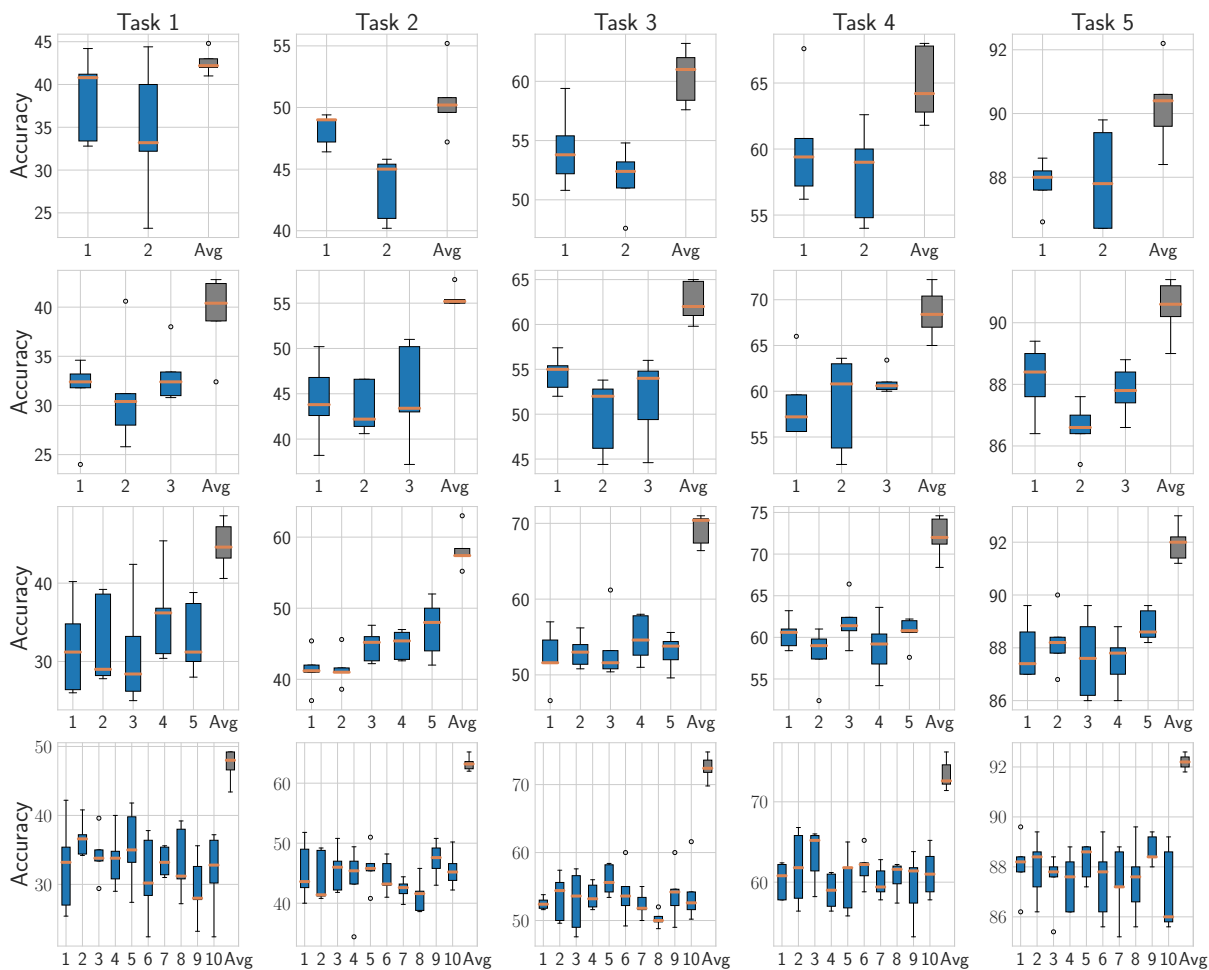


Figure 11: Final accuracy for each model of the ensemble (blue) and the final ensemble prediction (gray) for each task for Split CIFAR-100. Note how the ensemble accuracy (grey) is almost always much better than the accuracy of the best member (blue).

D.4 Curvature of the solutions

We provide additional Hessian spectrum results at different training time (ω_τ^* , $\tau = 1, 2, 3$) from the perspective of task 1’s loss in Figure 12. Recall that the ensemble methods has similar Hessian spectrum as the single model (number of model $n = 1$ below) since they are trained independently and their loss averaged. We observe that subspace method has much lower eigenvalues as we increase the number of models compared to the single model (and hence ensemble). The Hessian spectrum describes the flatness of the solution learned and characterizes its variation magnitude (Dinh et al., 2017; Mirzadeh et al., 2020b). A small eigenvalue induces less variation of task 1’s loss when learning subsequent task (2nd and 3rd columns).

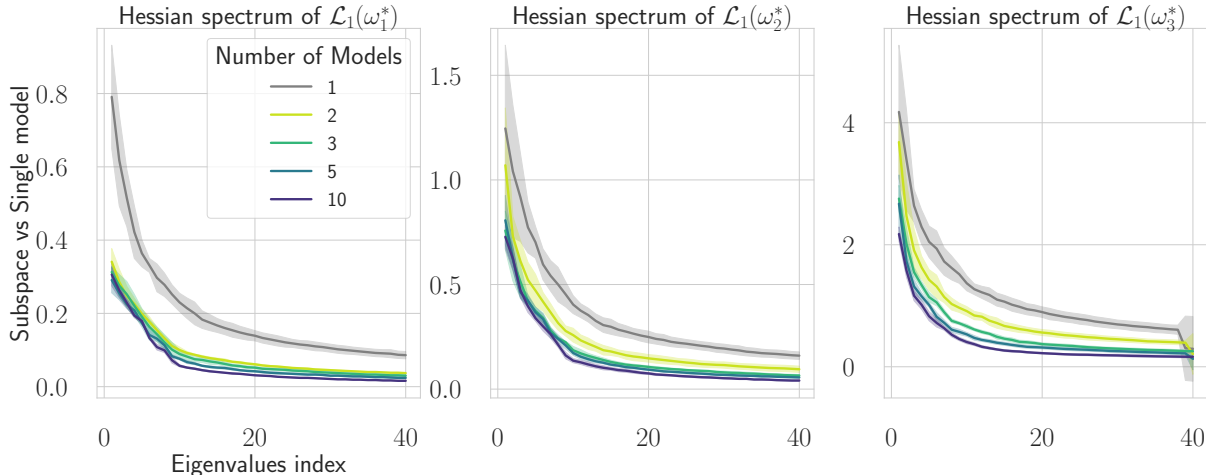


Figure 12: Hessian spectrum on Rotated MNIST throughout the training. Subspace methods have smaller eigenvalues which translate into flatter solutions’ minima and less catastrophic forgetting.

D.5 Robustness to noise perturbation in the weight space

In this section, we assess the loss landscape through noise perturbation in the neighborhood of a solution’s minimum. We perturb each model weights with a multiplicative noise $\mathcal{N}(1, \sigma)$ since it scales well with the magnitude of each weight.

We perturb each model endpoint with a multiplicative noise to get a new weights $\omega'_{i*} \leftarrow \omega_{i*} * \mathcal{N}(1, \sigma), \forall i = 1 \dots n$ and evaluate the performance with that new set of weights. The process is repeated 5 times and results are averaged. The range of noise σ used are: $\sigma \in \{0.25, 0.5, 1.0, 1.25\}$ (Rotated MNIST) and $\sigma \in \{0.05, 0.1, 0.25, 0.5\}$ (Split CIFAR-100).

Fig 13 and 14 show the impact of noise perturbation in the weight space on the accuracy. This immediately shows on both datasets that midpoint always has better performance than endpoints. Increasing the number of model n increases the gap between midpoint and endpoint’s accuracy (Compare $n = 2, 3$ versus $n = 10$).

Next, we compare the robustness against ensemble methods (Fig 15). The gap is higher between subspace and ensemble methods (compare subspace with $n = 3$ versus ensemble with $n = 10$). One reason might be that subspace methods learn a region of low loss while ensemble methods rely only on a single independent solution’s minima.

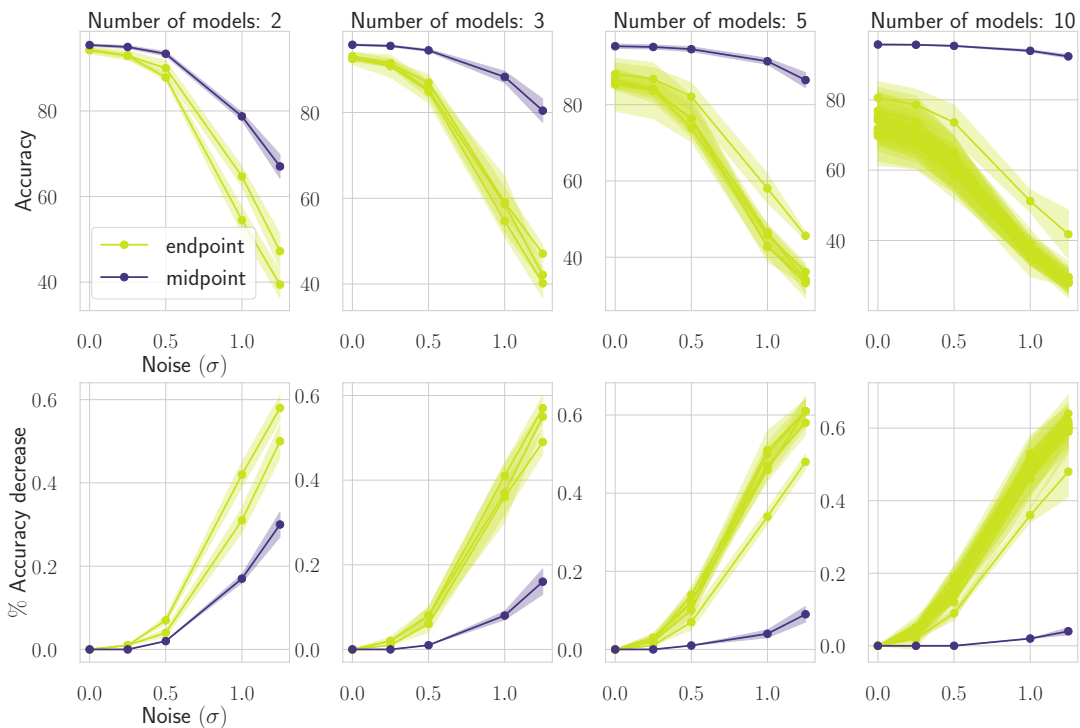


Figure 13: Robustness to multiplicative (uniform) noise Rotated MNIST- midpoint versus endpoints

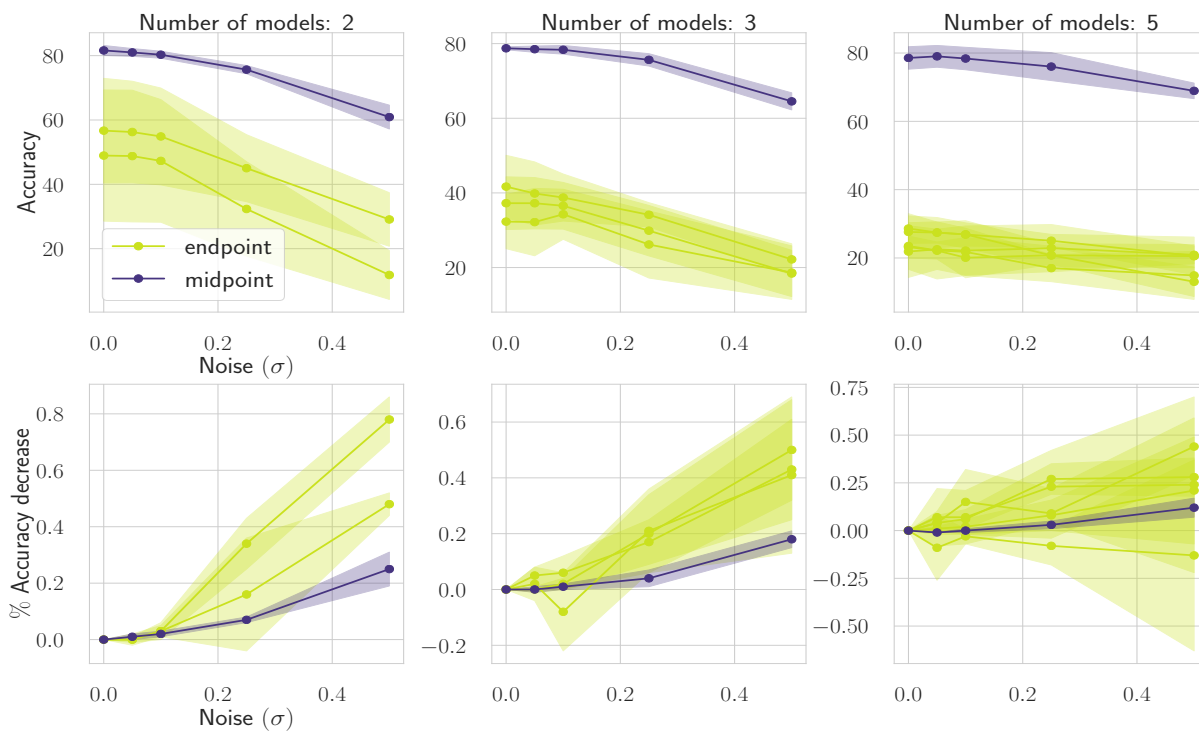


Figure 14: Robustness to multiplicative (uniform) noise Split CIFAR-100 - midpoint versus endpoints

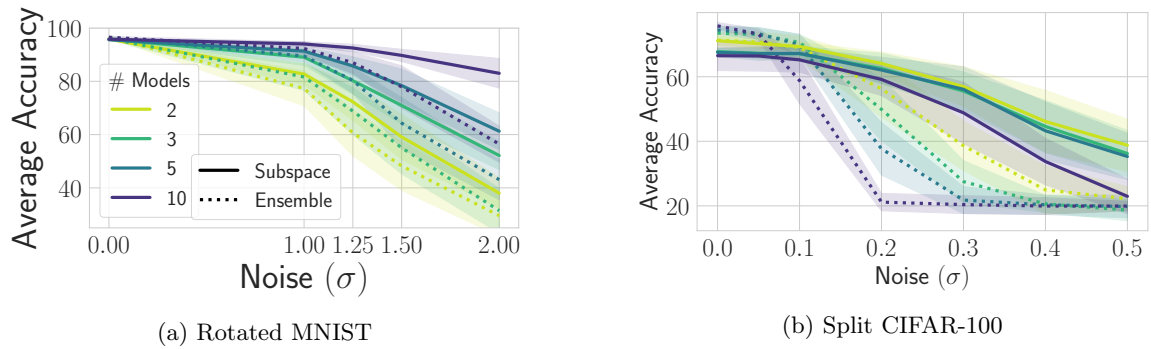


Figure 15: Robustness to noise on task 1 - Subspace versus Ensemble

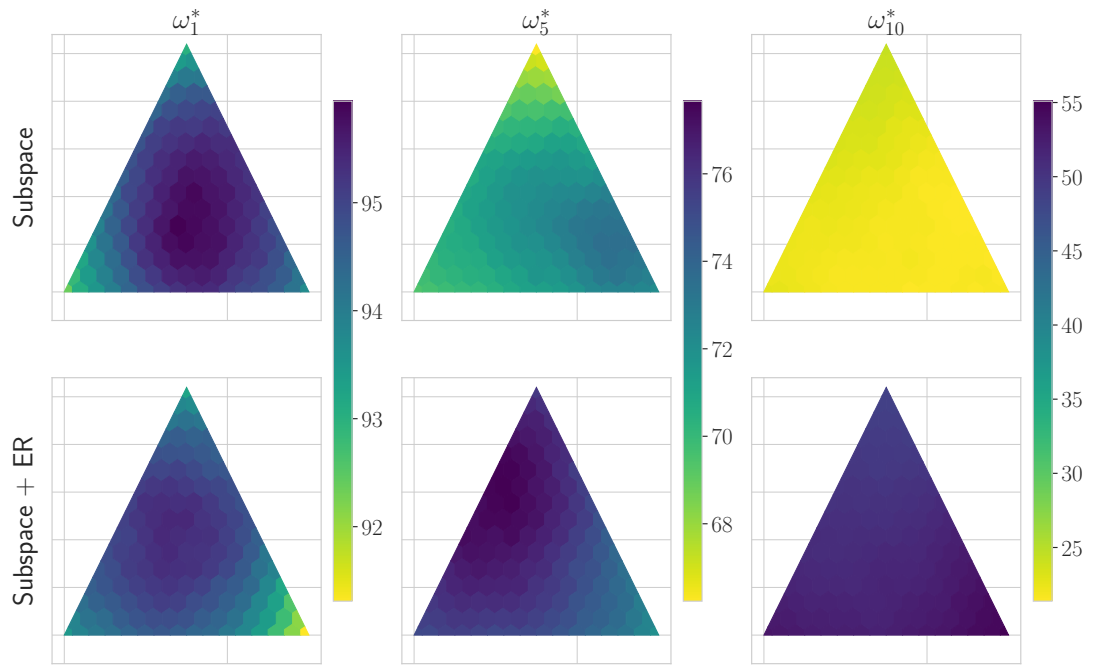


Figure 16: Evolution of accuracy of task 1 throughout the training. Even though subspace might constraint weight's movement, there is still a performance decrease.

D.6 Understanding subspace properties

This section aims at showing the dynamic of subspace through the training process.

D.6.1 Subspace connectivity

To measure the mode connectivity (Mirzadeh et al., 2021b) between subsequent solutions, we evaluate the loss function between interpolated solutions $\alpha\omega_i^* + (1 - \alpha)\omega_{i+1}^*, \forall \alpha \in [0, 1]$. Fig 17 provides a comparison between our method Subspace-Connectivity against Subspace CL (Alg. 4) and Subspace + ER (Alg. 5). We clearly see that the two latter incurs a high variation in their loss and accuracy between successive solutions on task 1's loss. As an example, while Subspace-Connectivity incurs a slight variation of 1% in accuracy when interpolating between ω_2^* and ω_3^* (2nd column) the other methods incur a drop of more than 2% of accuracy. This drop is even larger when interpolating between ω_3^* and ω_4^* (3rd column). Now we are interested to investigate the mode connectivity for further task's solution of Subspace-Connectivity .

Figure 18 shows the linear connectivity between solutions more than 5 tasks further in time. Although performance might have decreased between ω_{11}^* and ω_2^* on task 1, we can see that the linear path between ω_{11}^* and ω_{12}^* (red line) is close to horizontal losing roughly 2% of accuracy (first column) and 1% if one considers the path between ω_6^* and ω_7^* (green line). Note the high accuracy of $\omega_6^* \rightarrow \omega_7^*$ on task 1 (first column, green line) which reaches $\sim 94\%$ of accuracy while the accuracy of the first task (with ω_1^*) was around 96%.

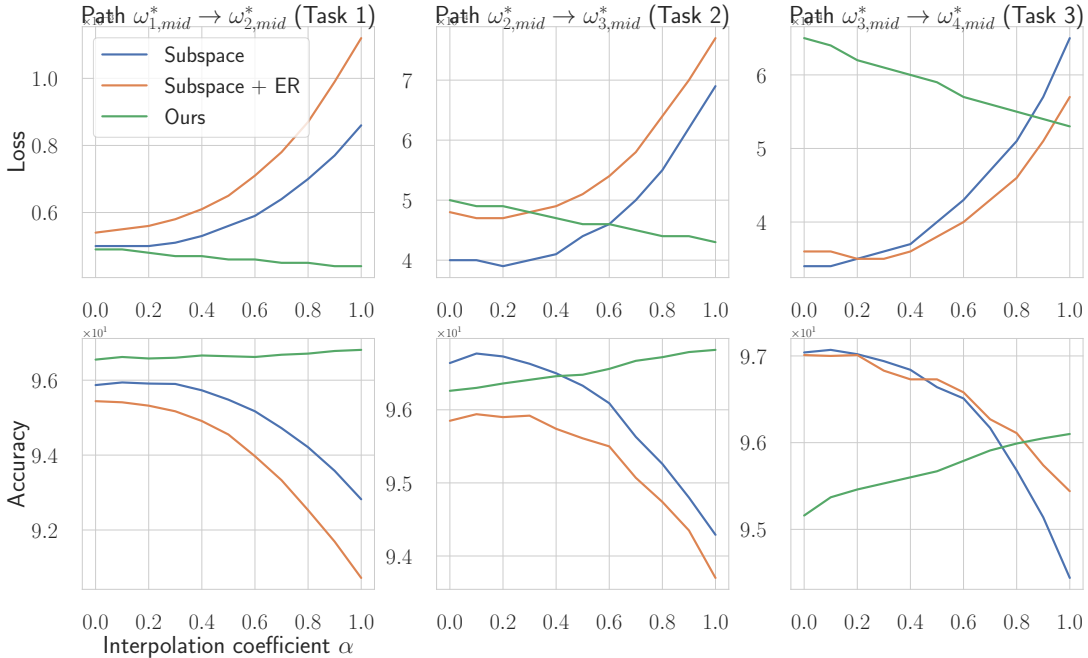


Figure 17: Connectivity comparison between Subspace-Connectivity and other baselines. Naive and ER+Subspace incurs high variation when interpolating between successive solutions since they do not enforce mode connectivity.

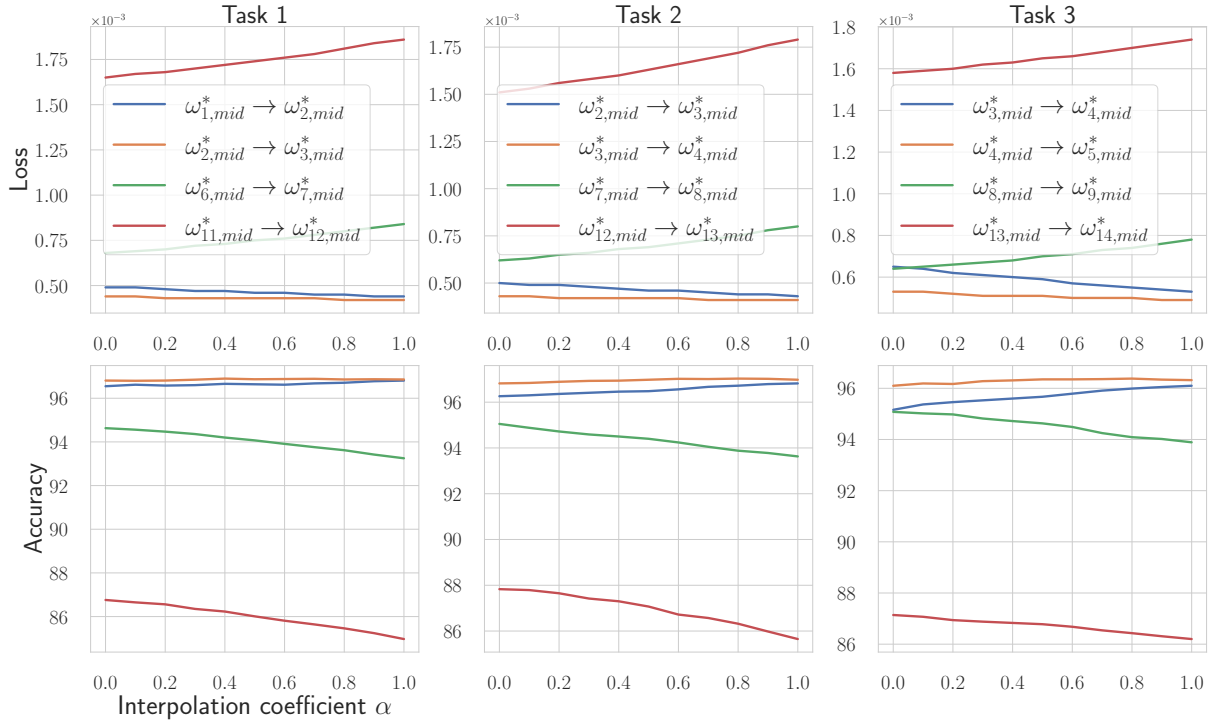


Figure 18: Subsequent solutions of Subspace-Connectivity maintain more or less connectivity (horizontality of each curve).

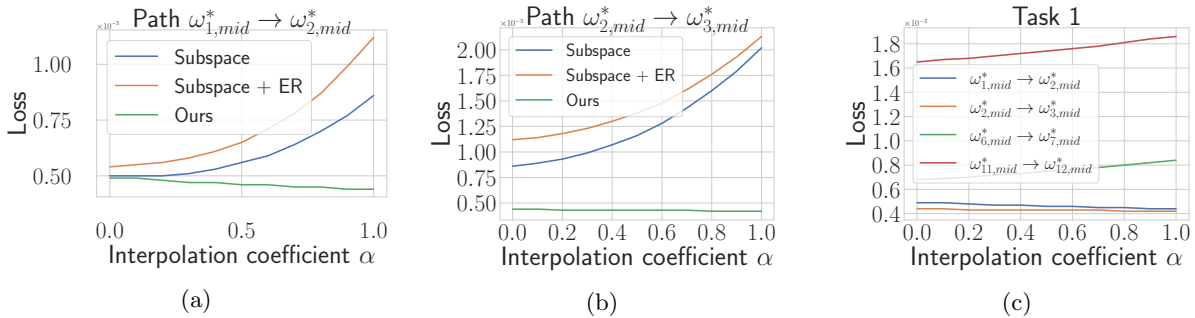


Figure 19: While applying naively subspace (Subspace and Subspace + ER) does not allow mode connectivity (loss function is increasing between two subsequent solutions) (left), our method (denoted "Ours") allows linear mode connectivity between successive solution'.

E Baselines hyperparameters

We first enumerate the hyperparameters used for the 20 tasks experiments in Table 1 before describing in detail the ablation in this section.

E.1 Hyper-Parameters

For the experiment in Section 5, we have used the following grid for each model. We note that for other algorithms (e.g., A-GEM, and EWC), we ensured that our grid contains the optimal values that the original papers reported. If applicable, all baselines used a buffer memory of 1 element per class per task (which translates in a total replay buffer memory of 200 for MNIST dataset and 100 for CIFAR-100 and miniImageNet). We used the same single training epoch per task setting as in (Chaudhry et al., 2019b; Mirzadeh et al., 2020b,a).

Naive SGD

- learning rate: [0.25, **0.1** (MNIST), **0.03** (miniImageNet), **0.01** (CIFAR-100), 0.001]
- batch size: 10

EWC

- learning rate: [0.25, **0.1** (MNIST, CIFAR-100), 0.01, 0.001]
- batch size: [64, **10**]
- λ (regularization): [100, **10** (MNIST, CIFAR-100), 1]

A-GEM

- learning rate: [0.1, **0.1** (MNIST), **0.01** (CIFAR-100), 0.001]
- batch size: [64, **10**]

ER-Reservoir

- learning rate: [0.25, **0.1** (MNIST, miniImageNet), **0.01** (CIFAR-100), 0.001]
- batch size: [64, **10**]

Stable SGD

- initial learning rate: [0.25, **0.1** (MNIST, CIFAR-100), 0.01, 0.001]
- learning rate decay: [0.95, **0.9**(CIFAR-100), 0.85,0.8 (miniImageNet), **0.6**(MNIST)]
- batch size: [64, **10**]
- dropout: [**0.25** (MNIST), 0.1,**0.0** (CIFAR-100, miniImageNet)]

Mode Connectivity SGD

To obtain continual minima (i.e., $\hat{\omega}_1^*$ to $\hat{\omega}_{20}^*$), we use the following hyperparameters:

- initial learning rate: [0.25, **0.1** (MNIST, CIFAR-100), 0.01, 0.001]
- momentum: [0.9, 0.85, **0.8** (MNIST), **0.7** (miniImageNet), **0.4** (CIFAR-100)]
- learning rate decay: [**0.95** (Rotated MNIST, CIFAR-100), **0.9** (miniImageNet), 0.85, **0.8** (Permuted MNIST), 0.7]
- batch size: [**64** (MNIST), 32, **10** (CIFAR-100, miniImageNet)]
- dropout: [**0.25** (Permuted MNIST), 0.1, **0.0** (Rotated MNIST, CIFAR-100, miniImageNet,)]

To obtain $\bar{\omega}_1^*$ to $\bar{\omega}_{20}^*$, we use the following grid:

- number of samples: [10, **5**, 3] for both MNIST and CIFAR experiments.
- learning rate: [0.2, 0.1, **0.05** (MNIST), **0.01** (CIFAR-100), 0.001].

Subspace-Connectivity

To obtain the subspace solution from the first step $\{\hat{\omega}_i^*\}_{i=1}^n$ from Eq 4.1, we used the following hyperparameters:

- initial learning rate: [**0.3**⁷ (CIFAR-100), 0.2, **0.15** (miniImageNet) , **0.1** (MNIST)]
- momentum: [0.9, 0.85, **0.8** (Rotated MNIST), **0.4** (Permuted MNIST), **0** (CIFAR-100, miniImageNet)]
- learning rate decay: [**0.95** (Rotated MNIST, CIFAR-100, miniImageNet), 0.9, **0.8** (Permuted MNIST)]
- batch size: [32, **10** (MNIST, CIFAR-100, miniImageNet)]
- dropout: [**0.25** (Permuted MNIST), 0.1, **0.0** (Rotated MNIST, CIFAR-100, miniImageNet)]

⁷this value must be multiplied by the number of model n to get the final learning rate used. Same logic is applied for miniImageNet dataset.

The subspace connectivity steps leading to $\{\omega_i^*\}_{i=1}^n$ (Eq 4.2) used the following hyperparameters:

- number of samples: [10, **5** (MNIST), **3** (CIFAR-100, miniImageNet)]
- learning rate: [0.2, **0.1** (CIFAR-100), **0.05** (MNIST, miniImageNet),].

Implementation details of Subspace-Connectivity While the first loss (Eq. 4.1) is a fine-tuning on the incoming task $\tau - 1$ (Vanilla SGD), the second one (Eq. 4.2) is done in two steps. First, we initialize the weight using a convex combination of weights around the two former midpoints as $\bar{\omega}_i = \alpha \omega_{\tau-1, mid}^* + (1 - \alpha) \hat{\omega}_{\tau, mid}$ then we add multiplicative noise $\bar{\omega}_i * \epsilon$, $i = 1 \dots n$, $\epsilon \sim \mathcal{N}(1, \sigma)$ (with $\sigma = 0.005$ for MNIST and $\sigma = 0.01$ for CIFAR-100 and miniImageNet) where $*$ represents element-wise multiplication. The multiplicative noise has the nice property to scale well with the weights magnitude. The α values taken are: [0.9, **0.85** (Rotated MNIT), **0.8** (CIFAR-100), **0.7** (miniImageNet), **0.25** (Permuted MNIST),]

F Additional results and setup details

In this section, we first provide our experimental setup and benchmarks used. We then check if our method connects the subspace of previous solutions together and finally compare our algorithm Subspace-Connectivity against the main baselines of the literature.

F.1 Experimental setup

Setup The experimental setup, such as benchmarks, network architectures, continual learning setting (e.g., number of tasks, episodic memory size, and training epochs per task), hyper-parameters, and evaluation metrics are chosen to be similar to several other studies (Chaudhry et al., 2019a; Mirzadeh et al., 2020b; Chaudhry et al., 2019b; Farajtabar et al., 2020). For all experiments, we report the average and standard deviation over five runs with different random seeds.

Benchmarks We use the standard benchmarks similarly to Goodfellow et al. (2014a) and Chaudhry et al. (2019b). Permuted-MNIST (Goodfellow et al., 2014a) consists of a series of MNIST supervised learning tasks, where the pixels of each task are permuted with respect to a fixed permutation. Rotation-MNIST (Farajtabar et al., 2020) consists of a series of MNIST classification tasks, where the images are rotated with respect to a fixed angle, monotonically. We increment the rotation angle by 9 degrees at each new task. Split CIFAR-100 (Chaudhry et al., 2019b) is constructed by splitting the original CIFAR-100 dataset (Krizhevsky et al., 2009) into 20 disjoint subsets. In order to assess the robustness to catastrophic forgetting over long tasks sequences, all datasets have 20 tasks. Split miniImageNet is a variant of the ImageNet dataset (Russakovsky et al., 2015), also splitted in 20 disjoint subsets where each subset is formed by sampling without replacement of 5 classes out of 100. Both CIFAR-100 and miniImageNet contains 20 tasks with 500 samples for each of the 5 classes.

Architectures For MNIST dataset, we used a fully connected neural networks with two hidden layers of 256 ReLU hidden units as in Chaudhry et al. (2019a); Mirzadeh et al. (2020b); Chaudhry et al. (2019b); Farajtabar et al. (2020). For Split CIFAR-100, we used the same reduced Resnet18 as in (Mirzadeh et al., 2020b) (with three times less features maps accros all layers). For Split miniImageNet, we adapted the network used with CIFAR-100 by adapting the input dimension of the last fully connected layers since both dataset have different input dimensions ((3,84,84) for miniImageNet versus (3,32,32) for CIFAR-100).

Evaluation metrics To assess the performance of each baseline, we report two metrics used in the literature which are the **Final Accuracy** and **Forgetting Measure**. The Final Accuracy after T tasks is the average validation accuracy over all the tasks $\tau = 1 \dots T$ defined as: $A_T = \frac{1}{T} \sum_{\tau=1}^T a_{T,\tau}$ where $a_{T,\tau}$ is the validation accuracy of task τ after the model finished learning on task T . The Forgetting Measure is defined as: $F_T = \frac{1}{T-1} \sum_{\tau=1}^{T-1} \max_{t=\{1..T-1\}} (a_{t,\tau} - a_{T,\tau})$

F.2 Comparison against larger models

This section provides ablation performance between MC-SGD, Ensemble MCSGD and Subspace-Connectivity with varying number of parameters and models n .

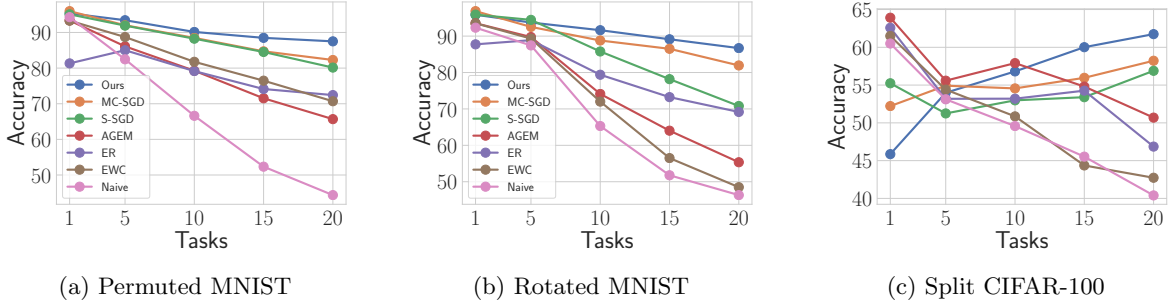


Figure 20: Evolution of the average accuracy throughout the training.

- Table 3 shows the performance for Subspace-Connectivity with different number of models n
- Table 4, 5 and 7 compare Subspace-Connectivity against Scaled single model and Ensemble MC-SGD varying: number of models n , parameters and for different level of compute cost (FLOPS).
- Table 6 compares two strategies of ensemble MC-SGD (bagging and training independently) with varying number of models n
- Table 8 compares Subspace-Connectivity against single model baselines of the literature
- Figure 21 showcases the trade-off between performance and computational efficiency of MC-SGD, Ensemble MC-SGD and Subspace-Connectivity for varying number of parameters and models n

In this section, we compare the performance of subspace method against the ensemble method and scaled single model. Scaled single models are augmented with a higher number of hidden units (MNIST) or filters (Split CIFAR-100, Split miniImageNet). The goal is to highlight the impact of the number of parameters versus the strategy used (ensemble, subspace, single model).

Scaled single model In order to compare to the performance on a single model ($n = 1$), we increase its capacity to match the number of parameters of the ensemble methods. While fully connected networks (MNIST dataset), we increase the number of hidden units ($h = 256, 450, 600$), for the Resnet18 network (Split CIFAR-100), we increase the number of channels ($nf = 20, 29, 35$).

Calculation of the FLOPS The Floating Point Operation per Second is a metric to quantify the computational cost for an algorithm. Our reported FLOPS metric represents a forward pass cost given a batch size of 10. To have an idea of the total training cost, one can approximate the backward pass as ~ 2 times the forward pass cost.

Number of model	Permuted MNIST		Rotated MNIST		Split CIFAR-100		Split miniImageNet	
	Accuracy \uparrow	Forgetting \downarrow	Accuracy \uparrow	Forgetting \downarrow	Accuracy \uparrow	Forgetting \downarrow	Accuracy \uparrow	Forgetting \downarrow
2	87.1 (± 0.19)	0.07 (± 0.01)	86.6 (± 0.45)	0.07 (± 0.01)	60.97 (± 1.53)	0.05 (± 0.01)	57.10 (± 1.53)	0.05 (± 0.01)
3	87.8 (± 0.53)	0.06 (± 0.01)	86.7 (± 0.67)	0.07 (± 0.01)	61.74 (± 0.80)	0.05 (± 0.01)	58.17 (± 0.84)	0.03 (± 0.01)
5	87.8 (± 0.3)	0.07 (± 0.01)	86.8 (± 0.46)	0.07 (± 0.01)	60.85 (± 0.73)	0.05 (± 0.01)	58.11 (± 1.23)	0.03 (± 0.01)

Table 3: Final accuracy for subspace method with a different number of models n . For $n \geq 2$ models, there is not much difference in performance for MNIST dataset while for Split CIFAR-100, $n = 3$ gives the best performance.

Number of model	Permuted MNIST		Rotated MNIST		FLOPS (1e6)	Relative FLOPS ratio
	Accuracy \uparrow	Forgetting \downarrow	Accuracy \uparrow	Forgetting \downarrow		
$ \theta = 268K$						
MC-SGD (256)	83.17 (± 0.63)	0.10 (± 0.01)	81.70 (± 0.43)	0.08 (± 0.01)	2.70	1
$ \theta = 560K$						
MC-SGD (450)	86.80 (± 0.93)	0.07 (± 0.01)	82.67 (± 0.20)	0.08 (± 0.01)	5.62	2.1
Ensemble MC-SGD ($n = 2$, bagging*)	86.23 (± 0.52)	0.06 (± 0.01)	80.7 (± 0.50)	0.09 (± 0.01)	2.70	1
Ensemble MC-SGD ($n = 2$)	86.5 (± 0.33)	0.08 (± 0.01)	83.00 (± 0.45)	0.08 (± 0.01)	5.4	2
Subspace-Connectivity ($n = 2$)	87.1 (± 0.19)	0.07 (± 0.01)	86.6 (± 0.45)	0.07 (± 0.01)	2.96	1.1
$ \theta = 836K$						
MC-SGD (600)	88.03 (± 0.36)	0.06 (± 0.01)	83.67 (± 0.40)	0.07 (± 0.01)	8.39	3.1
Ensemble MC-SGD ($n = 3$, bagging)	86.60 (± 0.46)	0.05 (± 0.01)	80.00 (± 0.24)	0.08 (± 0.01)	2.70	1
Ensemble MC-SGD ($n = 3$)	88.30 (± 0.48)	0.06 (± 0.01)	83.63 (± 0.39)	0.07 (± 0.01)	8.10	3
Subspace-Connectivity ($n = 3$)	87.8 (± 0.30)	0.07 (± 0.01)	86.7 (± 0.67)	0.07 (± 0.01)	3.26	1.2

Table 4: Comparison against models with larger parameters. While for MC-SGD number in bracket refers to the hidden units number, for ensemble and subspace methods it refers to the number of model n . * For the bagging method, every time a data batch arrives, we sample uniformly one model among the other to receive the data and be updated. This reduces the computational cost to be similar to the single model but with each of the n models receiving $1/n$ -th of the whole dataset.

Number of model	Split CIFAR-100		FLOPS (1e8)	Relative FLOPS ratio
	Accuracy \uparrow	Forgetting \downarrow		
$ \theta = 500K$				
MC-SGD ($nf = 20$)	58.22 (± 0.91)	0.08 (± 0.01)	2.60	1
$ \theta = 1M$				
MC-SGD ($nf = 29$)	60.12 (± 0.97)	0.07 (± 0.01)	5.38	2.01
Ensemble MC-SGD ($n = 2$, bagging)	56.87 (± 0.80)	0.06 (± 0.01)	2.60	1
Ensemble MC-SGD ($n = 2$)	60.83 (± 0.99)	0.09 (± 0.01)	5.20	2
Subspace-Connectivity ($n = 2$)	60.97 (± 1.53)	0.05 (± 0.01)	2.60	~ 1.00
$ \theta = 1.5M$				
MC-SGD ($nf = 35$)	60.50 (± 0.84)	0.06 (± 0.01)	7.78	3
Ensemble MC-SGD ($n = 3$, bagging)	55.48 (± 1.20)	0.06 (± 0.01)	2.60	1
Ensemble MC-SGD ($n = 3$)	64.12 (± 1.16)	0.06 (± 0.01)	7.80	3
Subspace-Connectivity ($n = 3$)	61.74 (± 0.80)	0.05 (± 0.01)	2.60	~ 1.00
Subspace-Connectivity ($n = 3, k = 2^*$)	65.90 (± 1.23)	0.07 (± 0.01)	5.20	~ 2.00

Table 5: Comparison against models with larger parameters. While for MC-SGD number in bracket refers to the number of channels for the Resnet18 architecture, for ensemble and subspace methods it refers to the number of model n . * To match the ensemble methods compute cost, we increased the training epoch to 2 hence incurring twice the training cost.

Method	Permuted MNIST		Rotated MNIST		Split CIFAR-100		Split miniImageNet	
	Accuracy \uparrow	Forgetting \downarrow	Accuracy \uparrow	Forgetting \downarrow	Accuracy \uparrow	Forgetting \downarrow	Accuracy \uparrow	Forgetting \downarrow
bagging strategy (same compute as single model)								
Ensemble MC-SGD ($n=2$)	86.23 (± 0.52)	0.06 (± 0.01)	80.7 (± 0.50)	0.09 (± 0.01)	56.87 (± 0.80)	0.06 (± 0.01)	54.00 (± 0.77)	0.05 (± 0.01)
Ensemble MC-SGD ($n=3$)	86.60 (± 0.46)	0.05 (± 0.01)	80.00 (± 0.24)	0.08 (± 0.01)	55.48 (± 1.20)	0.06 (± 0.01)	52.39 (± 0.60)	0.03 (± 0.01)
Ensemble MC-SGD ($n=4$)	85.37 (± 0.15)	0.05 (± 0.01)	78.53 (± 0.19)	0.09 (± 0.01)	54.44 (± 1.16)	0.07 (± 0.01)	51.37 (± 0.66)	0.04 (± 0.01)
Ensemble CL (n times more compute)								
Ensemble MC-SGD ($n=2$)	86.5 (± 0.33)	0.08 (± 0.01)	83.00 (± 0.45)	0.08 (± 0.01)	60.83 (± 0.99)	0.09 (± 0.01)	57.60 (± 0.55)	0.04 (± 0.01)
Ensemble MC-SGD ($n=3$)	88.30 (± 0.48)	0.06 (± 0.01)	83.63 (± 0.39)	0.07 (± 0.01)	64.12 (± 1.16)	0.06 (± 0.01)	59.10 (± 1.1)	0.04 (± 0.01)
Ensemble MC-SGD ($n=4$)	88.54 (± 0.65)	0.06 (± 0.01)	83.6 (± 0.20)	0.08 (± 0.01)	64.84 (± 1.10)	0.06 (± 0.01)	59.80 (± 1.03)	0.04 (± 0.01)

Table 6: Ensemble performance for a different number of models (n) and strategies.

Number of model	Split miniImageNet		FLOPS (1e8)	Relative FLOPS ratio
	Accuracy \uparrow	Forgetting \downarrow		
$ \theta = 500K$				
MC-SGD ($nf = 20$)	54.80 (± 1.04)	0.05 (± 0.01)	18.31	1
$ \theta = 1M$				
MC-SGD ($nf = 29$)	55.30 (± 0.83)	0.06 (± 0.01)	37.85	2.06
Ensemble MC-SGD ($n = 2$, bagging)	54.00 (± 0.77)	0.05 (± 0.01)	18.31	1
Ensemble MC-SGD ($n = 2$)	57.60 (± 0.55)	0.04 (± 0.01)	36.62	2
Subspace-Connectivity ($n = 2$)	57.10 (± 0.79)	0.05 (± 0.01)	18.31	~ 1.00
$ \theta = 1.5M$				
MC-SGD ($nf = 35$)	55.44 (± 1.36)	0.05 (± 0.01)	54.77	3
Ensemble MC-SGD ($n = 3$, bagging)	52.39 (± 0.60)	0.03 (± 0.01)	18.31	1
Ensemble MC-SGD ($n = 3$)	59.1 (± 1.1)	0.04 (± 0.01)	54.92	3
Subspace-Connectivity ($n = 3$)	58.17 (± 0.84)	0.03 (± 0.01)	18.32	~ 1.00

Table 7: Comparison against models with larger parameters for Split miniImageNet.

Method	Split miniImageNet	
	Accuracy \uparrow	Forgetting \downarrow
Naive SGD	43.66 (± 1.65)	0.22 (± 0.02)
ER Reservoir (Chaudhry et al., 2019b)	51.7 (± 2.53)	0.11 (± 0.02)
Stable SGD (Mirzadeh et al., 2020b)	53.76 (± 1.13)	0.07 (± 0.01)
MC-SGD (Mirzadeh et al., 2021b)	54.80 (± 1.04)	0.05 (± 0.01)
Subspace-Connectivity (ours)	58.17 (± 0.84)	0.03 (± 0.01)
Multitask Learning	62.82 (± 1.77)	0.0

Table 8: Comparison between Subspace-Connectivity and other baselines on 5 random seeds for Split miniImageNet. Although, we increase the number of model n for Subspace-Connectivity, it still has a training cost similar to the single model yet enjoying good performance. As an example, Ensemble MC-SGD ($n = 3$) only improves over of $\sim 1\%$ but incurs three times more computational cost.

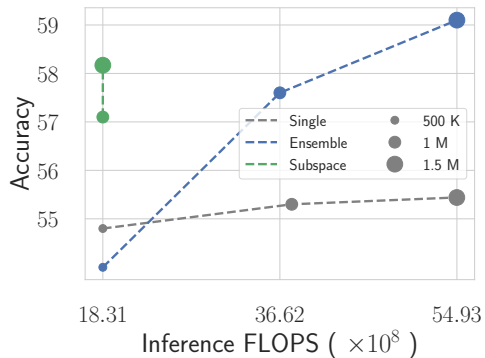


Figure 21: Performance of MC-SGD (Single), Ensemble MC-SGD (Ensemble) and Subspace-Connectivity (Subspace) with respect to the inference cost (FLOPS) and number of parameters/models n (circles) for Split miniImageNet. Overall Ensemble MC-SGD with $n = 3$ models is improving performance over Subspace-Connectivity of only 1.5% but at the cost of 3 times more compute. This makes our method computationally efficient while keeping a good performance.